VOLTAGE-DRIVEN BIOCATALYSIS BY

MEMBRANE-BOUND LIVER ENZYMES

By

RAJASEKHARA REDDY NERIMETLA

Bachelor of Science
Sri Kirshnadevaraya University
Anantapur, Andhra Pradesh
2007

Master of Science in Chemistry
Banaras Hindu University
Varanasi, Uttar Pradesh
2010

Submitted to the Faculty of the
Graduate College of the
Oklahoma State University
in partial fulfillment of
the requirements for
the Degree of
DOCTOR OF PHILOSOPHY
July, 2017

VOLTAGE-DRIVEN BIOCATALYSIS BY

MEMBRANE-BOUND LIVER ENZYMES

Dissertation Approved:

Dr. Sadagopan Krishnan

Dissertation Adviser

Dr. Richard A. Bunce

Dr. Ziad El Rassi

Dr. Christopher J. Fennell

Dr. Ranjith Ramanathan

Outside Committee Member Name Here

ACKNOWLEDGEMENTS

I would like to express my deepest appreciation to my advisor Dr. Sadagopan Krishnan. Without his guidance and support this thesis would not have been possible. Thank you for all your enthusiasm, optimism and encouragement. It was definitely a great learning experience.

I would like to thank Dr. Ziad El Rassi, Dr. Richard A. Bunce, Dr. Christopher J. Fennell and Dr. Ranjith Ramanathan for their valuable inputs and suggestions.

I would like to thank the Department of Chemistry for supporting me during my graduate studies at Oklahoma State University by providing a teaching assistantship. I would like to thank Dr. Sadagopan Krishnan for giving me a research assistantship. I would like to express my gratitude to all the faculty and staff for their helpfulness whenever needed.

Ultimately and most importantly, I would like to dedicate this work to my parents Sanjeeva Reddy and Thimmakka Reddy Nerimetla and my beloved wife Keerthi Reddy Nerimetla. My deepest gratitude to my loving brothers Kastura Reddy and Bhaskar Reddy for their support. A special thanks to my in-laws Mr. and Mrs. Lakshmi Reddy and Jaya Prameela Reddy Konduru for all the support and love. This achievement is mine but certainly not without the contribution of all the mentioned and unmentioned people

Name: RAJASEKHARA REDDY NERIMETLA

Date of Degree: JULY, 2017

Title of Study: VOLTAGE-DRIVEN BIOCATALYSIS BY MEMBRANE-BOUND LIVER ENZYMES

Major Field: CHEMISTRY

Abstract: Human liver microsomes (HLMs) contain the major drug metabolizing cytochrome P450 (CYP) enzyme, and their redox partner protein, CYP-NADPH reductase (CPR). Due to the broad range of biocatalytic reactions catalyzed by CYP enzymes, chemists have focused on the structure-function, biosensing, and catalytic applications of this unique class of enzymes. For drug development, HLMs are being used as the *in vitro* system to study drug metabolism, inhibition, isoform and metabolite profiling, biosensing applications, and drug-drug interactions. My research focus is to understand the electrocatalytic pathways of human and bacterial (bactosomes) membrane-bound liver CYP enzymes as a new bioelectronics platform for drug development and biosensing. We designed a biologically active bactosomal film on a self-assembled monolayer surface, and compared the electrocatalytic properties of CYP, CPR, and the combination of these two expressed in bactosomes. In addition, we developed a human liver microsomal bioreactor constructed on carbon nanostructure electrodes for applications in stereoselective drug metabolite synthesis. We extended this carbon nanostructure approach with magnetic nanomaterials to develop sensitive biosensors and volume-efficient electrocatalytic systems. My other short-term project was to utilize electrochemistry to understand meat color attributes based on redox properties of myoglobin from different species studied under various meat relevant pH conditions.

TABLE OF CONTENTS

Chapter **Page**

LIST OF TABLES

CHAPTER II

Table **Page**

CHAPTER IV

CHAPTER V

LIST OF FIGURES

CHAPTER II

Figure **Page**

CHAPTER III

CHAPTER IV

CHAPTER V

CHAPTER I

INTRODUCATION

The objective of this dissertation is to understand the electrocatalytic properties of bacterial expressed cytochrome P450 (CYP) enzymes and human liver microsomes on new carbon electrode designs and nanostructures. Additionally, the use of electrochemistry as a tool to study meat color attributes based on myoglobin from different species under various pH conditions is demonstrated.

Human cytochrome P450 (CYP) enzymes represent a major class of drug metabolizing monooxygenases present in several organs (e.g., liver, lungs, and esophagus). CYP enzymes have gained attention among the catalysis, biochemistry, biomedical, bioengineering, pharmaceutical, electrochemistry, and toxicology communities due to their unique and broad substrate specificities and their ability to catalyze many stereoselective biochemically and technologically valuable reactions (e.g., carbon hydroxylation, epoxidation, heteroatom oxygenation, and dealkylation).[1-7]

For drug development, human liver microsomes (HLM) are being used as in vitro systems to study drug metabolism, inhibition, and drug-drug interactions and to identify the specific isoforms of CYPs involved in these processes.[8] In the in vitro biological assays, NADPH used as an electron source delivered to reduce a CYP heme center mediated by reductase (CPR) via its flavin adenine dinucleotide (FAD) and flavin mononucleotide (FMN) cofactors.[9] Replacing NADPH with an electrode as an electron source to study the direct electron transfer and catalytic properties of genetically engineered microsomes, rat liver microsomes, and HLM assembled as films with polyions, microsomes coated on

different thiolated hydrophobic gold electrodes, and layer-bylayer films of purified human CYPs and microsomal CPR have been performed successfully.[10-13]

Chapter II presents the detailed mechanistic study of the electrocatalytic pathway of membranebound CPR-CYP, only CYP and only CPR. Voltage-driven membrane-bound CYP-catalyzed drug metabolite formation and quantification are demonstrated. Chapter III explores the electrocatalytic properties and reusability features of drug metabolizing human liver microsomes (HLM) adsorbed onto multiwalled carbon nanotubes (MWNT) coated on edge plane pyrolytic graphite electrodes (EPGs).

Chapter IV details the reduction and oxygenation kinetics of myoglobin at three different pH conditions (physiological state (pH 7.4), stressed animal muscle (pH 6.4), and post-mortem meat (pH 5.6) were examined in this study). The electrochemically estimated oxygen affinity by reduced myoglobin at various pH conditions correlated with the color of meat.

Chapter V investigates the species-specific effect (beef and pork) on metmyoglobin reduction potentials and oxygen affinity by cyclic voltammetry technique.

REFERENCES

1. Evans, W. E.; Relling, M. V. Science 1999, 286 (5439), 487-491.
2. Gilardi, G.; Fantuzzi, A.; Sadeghi, S. J. Curr. Opin. Struct. Biol. 2001, 11, 491-499.
3. Krishnan, S.; Schenkman, J. B.; Rusling, J. F. J. Phys. Chem. B. 2011, 115, 8371-8380.
4. Bistolas, N.; Wollenberger, U.; Jung, C.; Scheller, F. W. Biosens. Bioelectron. 2005, 20, 2408-2423.
5. Green, M. T. Curr. Opin. Chem. Biol. 2009, 13, 84-88.
6. Hagen, K. D.; Gillan, J. M.; Im, S. C.; Landefeld, S.; Mead, G.; Hiley, M.; Waskell, L. A.; Hill, M. G.; Udit, A. K. J. Inorg. Biochem. 2013, 129, 30-34.
7. Immoos, C. E.; Chou, J.; Bayachou, M.; Blair, E.; Greaves, J.; Farmer, P. J. J. Am.Chem. Soc. 2004, 126, 4934-4942.
8. Wienkers, L. C; Heath, T. G. Nat. Rev. Drug Discovery, 2005, 4, 825–833.
9. Guengerich, F. P. J. Biochem. Mol. Toxicol. 2007, 21, 163−168.
10. Sultana, N.; Schenkman, J. B.; Rusling, J. F. J. Am. Chem. Soc. 2005, 127, 13460−13461.
11. Krishnan, S.; Rusling, J. F. Electrochem. Commun. 2007, 9, 2359−2363.
12. Wasalathanthri, D. P.; Malla, S.; Faria, R. C.; Rusling, J. F. Electroanalysis 2012, 24, −2052.
13. Krishnan, S.; Wasalathanthri, D.; Zhao, L.; Schenkman, J. B.; Rusling, J. F. J. Am. Chem. Soc. 2011, 133, 1459 −1465.

CHAPTER II

MECHANISTIC INSIGHTS ON THE VOLTAGE-DRIVEN BIOCATALYSIS OF A CYTOCHROME P450 BACTOSOMAL FILM ON A SELF-ASSEMBLED MONOLAYRER

2.1 Introduction

Obtaining mechanistic insights on the electrocatalytic pathways of membrane-bound metalloenzymes is crucial for successfully designing viable enzyme bioelectrodes for catalysis and sensing applications. Among several catalytically important membrane-bound enzymes, human cytochrome P450 (CYP) enzymes represent a major class of drug metabolizing monooxygenases present in several organs (e.g., liver, lungs, and esophagus). CYP enzymes have gained attention among the catalysis, biochemistry, biomedical, bioengineering, pharmaceutical, electrochemistry, and toxicology communities due to their unique and broad substrate specificities and their ability to catalyze many stereoselective biochemically and technologically valuable reactions (e.g., carbon hydroxylation, epoxidation, heteroatom oxygenation, and dealkylation).[1-12]

The CYP biocatalytic cycle involves substrate binding to the enzyme active site, reduction of the CYP-heme by CYP reductase (CPR) that uses NADPH as the electron source, a second electron reduction step (either by CPR or by cytochrome b5 in some CYP isoforms), and two protonation steps leading to the formation of CYP-ferryloxy radical cation (Scheme 1). This strong

oxidant can oxygenate the bound substrate and regenerate the resting ferric-heme state of the enzyme for subsequent catalytic turnover.[13] In the case of isolated, soluble, and membrane-free CYPs, hydrogen peroxide (H_2O_2) can help to attain the active oxygenated form of CYPs (peroxide shunt pathway) for substrate monooxygenation.[14,15]

In contrast to human CYPs, bacterial CYPcam (the abbreviation "cam" denotes camphor binding protein) utilizes an iron-sulfur protein, putidaredoxin, as the redox partner to deliver electrons from NADH. In the case of mitochondrial CYP enzymes (e.g., mammalian CYPscc, sterol 27-hydroxylase or CYP 27A1), a non-heme iron-sulfur redox protein acts as the redox partner rather than NADPH CPR.[16] Electrochemically, the need for a NADPH source can be eliminated by supplying electrons from an electrode under an applied negative potential either directly to the CYP-heme site or via CPR mediation.[3,17-19]

Scheme 1. Proposed catalytic mechanism of human CYP enzymes.[20]

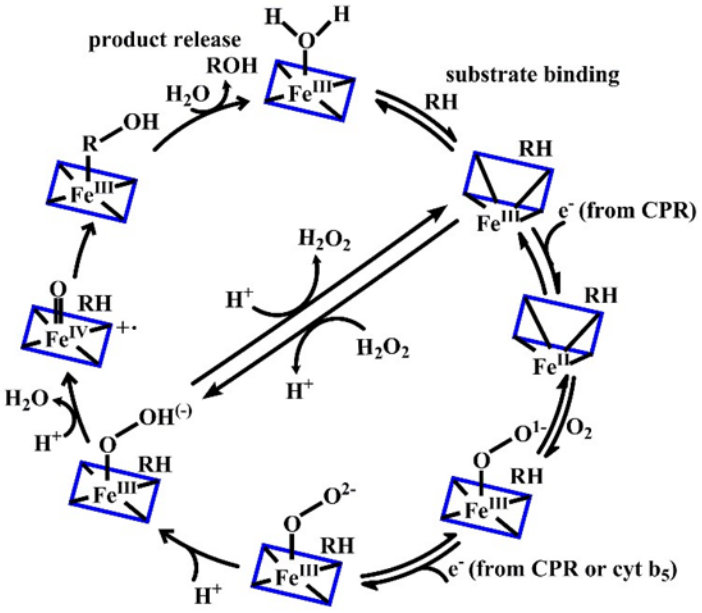

Representative electrochemical studies of films of various purified soluble CYP isoforms on electrodes include layer-by-layer films with polyions,14 CYPs mixed with surfactant films,[21-24]

various electrostatic film strategies,[25] covalent attachment onto a gold (Au) self-assembled monolayer (SAM),[26] and nanomaterial-modified electrodes.[27-29] Isolation and purification of CYP enzymes involves tedious and time-consuming procedures that often yield very low amounts of CYP, and additionally they require extensive care to obtain active forms of purified enzymes. Due to these limitations, our focus is on electrocatalytic studies of membrane-bound forms of bacterial expressed CYP with its reductase.

Estabrook et al. demonstrated the feasibility of electrochemically driving CYP catalysis in solution containing the dissolved heme domain of rat CYP 4A1 fused with the flavin domain of rat NADPH CPR in the presence of cobalt complex electron transfer mediators.[30,31] However, solution electrochemistry of proteins suffers from poor diffusion of large protein molecules to and from the electrode, electrode fouling by adsorbed inactive protein molecules, enzyme denaturation, associated charge transfer kinetic limitations, and difficulty in isolating product from the enzymatic solution for analysis. In contrast, protein film electrochemistry (PFE) is free of diffusion issues, as the protein is confined as a film at the electrode and efficient electron transport and electrocatalytic properties are possible via appropriate designs of electrodes for bioactive immobilization of enzymes.[10,32 ,33]

Successful PFE studies include genetically engineered membrane-bound forms of human CYP isoforms 1A2 and 3A4 with CPR (expressed in baculovirus-insect cells or E coli),17,18 membranebound CYPs present in rat liver microsomes,34 human liver microsomes adsorbed on various carbon electrodes and carbon nanostructures,[19,35,36] and layer-by-layer films of purified CYP 1A2 or 2E1 assembled with membrane-bound CPR on pyrolytic graphite electrodes.[37] Although CPR mediated CYP electrocatalysis was demonstrated, clear understanding of formal potentials and electrocatalytic pathways of membrane-bound films of CYP by themselves or in association with CPR is lacking.[18] To address this knowledge gap, this study focused on CYP 2C9

(or 3A4)+CPR, CYP 2C9, CPR, and control bactosomes (no CYP or CPR present) as electrostatically adsorbed films on cysteamine SAMs of Au infused quartz crystals.

Higher metabolite formation in the presence of peroxide-scavenging catalase suggested the minimization of membrane oxidative stress and the insignificance of a peroxide shunt pathway in the CYP bactosomal films. This is in contrast to the catalytic property of isolated, soluble, and membrane-free CYPs that utilize H_2O_2 for catalysis.[3,10,15] Moreover, formal potentials, oxygen reduction currents, and increased amounts of electrocatalytic diclofenac hydroxylation product confirmed the role of CPR in the CYP 2C9+CPR bactosomal film as the electron mediator from the electrode to the CYP 2C9-heme for catalysis. This quantitative bioelectrode construction method is simple, scalable (due to bacterial CYP expression systems for large scale CYP production with CPR), and useful for cost-effective, NADPH-free application of direct membranebound CYPs without the need for tedious isolation and purification of these enzymes to accomplish biocatalysis and for use in biosensing applications.

2.2 Experimental

2.2.1 Chemicals and materials

Catalase, cysteamine, and diclofenac were purchased from Sigma-Aldrich (St. Louis, MO, USA) and 4-hydroxydiclofenac was purchased from Cayman Chemicals (Ann Arbor, Michigan, USA). All other chemicals and reagents were analytical grade. For quartz crystal microbalance (QCM) measurements (Gamry Instruments, Warminster, PA, USA), Au infused quartz crystals (Au geometric area 0.2 cm^2, International Crystal Mfg., Oklahoma City, USA) operating at a fundamental oscillation frequency of 10 MHz were used.

CYP 2C9 expressed bactosomes with a residual CPR, CPR expressed bactosomes, CYP 2C9+CPR bactosomes, CYP 3A4+CPR bactosomes, and control bactosomes with no CYP or CPR were purchased from Cypex Ltd. (Dundee, Scotland, UK; US Distributor: Xenotech LLC, Kansas,

USA). Enzyme activities and protein concentrations in the bactosomes are provided in Table S1. As a representative case, we validated the supplier's specifications of CYP 2C9 content and activity using CO difference spectra and by the standard NADPH CYP assay (Supporting Information, Figure S1, and associated validation results).[37] Our results agreed with the supplier's specifications.

2.2.2 Instrumentation

QCM frequency changes and impedance spectroscopy measurements were made using an electrochemical quartz crystal microbalance (eQCM, Gamry Instruments) that interfaces a QCM with a potentiostat (Model: Interface 1000).[38-41] Electrochemical and electrocatalytic properties of bactosomal films were examined with a CH instrument (Model: CHI 6017, Austin, TX, USA). As the representative characterization, CYP 3A4+CPR bactosomes adsorbed onto the SAM of cysteamine on the Au surface, only the cysteamine modified surface, and only the bare Au surface were characterized by scanning electron microscopy (SEM, Model: FEI Quanta 600FE). Zeta potential measurements were made using a ZetaPALS potential analyzer (Brookhaven Instruments Corporation, Holtsville, NY, USA). High-performance liquid chromatography (HPLC, premier C18 column, length 10 cm, Dionex, Model: UltiMate 3000, ThermoFisher Scientific) was used to identify the products of electrolysis of diclofenac catalyzed by the bactosomal films. A mobile phase composition of 30% acetonitrile:70% water was delivered at a flow rate of 0.3 mL min^{-1}. Diclofenac and 4-hydroxydiclofenac peaks were identified based on chromatograms of standards run under similar conditions in the HPLC. Liquid chromatography-mass spectrometry (LC-MS) was performed using a 75-micron nano-LC column packed with 40 cm of C-18 beads (3 micron in diameter, MagicAQ beads from Bruker). A gradient elution was used proceeding from 100% mobile phase A (0.1% formic acid in water) to 80% mobile phase B (0.15% formic acid in acetonitrile). The column was eluted into the nanospray ion source of an LTQ-Orbitrap XL MS, and the mass spectra were collected in the FT mode using a nominal resolution of 60,000.

2.2.3 Electrochemical measurements

Electrochemical measurements were made in a standard three-electrode electrochemical cell consisting of an adsorbed bactosomal film on a cysteamine SAM on a Au infused quartz crystal as the working electrode, Ag/AgCl as the reference electrode, and a Pt wire as the counter electrode. Before performing cyclic voltammetry (CV) experiments for measuring redox potentials of the bactosomal films, 10 mL of phosphate buffer (pH 7.0) was argon purged for 30 min, and a constant argon atmosphere was maintained during measurements.

2.2.4 Electrostatic adsorption of CYP 2C9 or 3A4 bactosomes onto Au SAM surface

A cysteamine solution (10 mM in ethanol) at a flow rate of 15 μL min^{-1} was allowed to pass over the surface of Au infused quartz crystals for 30 min. The crystals were washed with buffer until a constant oscillation frequency was obtained. The surface amine end groups of the cysteamine SAM were used to adsorb negatively charged phospholipid membranes[19,34,42] of bactosomes (CYP 2C9, CPR, CYP 2C9+CPR, and CYP 3A4+CPR). As a representative case, zeta potential measurement of the CYP 2C9+CPR bactosomes in pH 7.0 indicated a negative surface charge with a value of −16.1 ± 1.8 mV (N = 3 replicates).

The vendor-supplied bactosomal solutions were 10-times diluted in phosphate buffer (pH 7.0), which was found to be an optimal dilution to use in the QCM flow channel system. The electrostatic binding was conducted at a flow rate of 15 μL min^{-1} for 30 min at room temperature.

For electrochemical studies, dilution of the bactosomes for adsorption onto the SAM Au quartz crystals is not required, so we used the bactosomes as supplied by the vendors. As controls, cysteamine SAM modified Au fused quartz crystals and those with adsorbed control bactosomes (with no CYP or CPR) were analyzed to estimate the non-enzymatic redox properties and to differentiate those from the electrocatalytic characteristics of the CYP and CYP+CPR bactosomal films.

2.2.5 Electrocatalytic oxygen reduction

Dioxygen is needed for CYP catalyzed reactions to form the reactive ferryloxy radical cation of CYP [+•(CYP-Fe^{IV}=O)] (Scheme 1). This oxoform helps oxygenate a CYP-specific substrate (e.g., diclofenac in our case). For dioxygen to bind to CYP, the reduction of CYP-Fe^{III}-heme to CYPFe^{II}-heme is necessary. This can be achieved electrochemically or by using chemical reducing agents.14 Under an applied negative potential in the absence of CYP substrate, the oxoform of CYP is reduced on electrodes to form H_2O_2, resulting in reduction currents with the regeneration of the resting ferric CYP-heme.[3,14] In the present study, the oxygen reduction catalyzed by the designed CYP and CPR bactosomal films was studied in stirred buffer solutions to achieve O2 mass transport by convection.[43] Control bactosomes, cysteamine SAM on Au, and bare Au infused quartz crystals were also tested for oxygen reduction properties to understand the contribution of CYP electrocatalytic activity in bactosomes.

2.2.6 Electrocatalytic diclofenac hydroxylation by the bactosomal films

Enzyme catalytic activity to convert drug compounds into metabolites is the main goal of constructing any CYP immobilized films on electrodes. To examine the catalytic activity of the bactosomal films (i.e., CYP 2C9, CPR, 2C9+CPR, and 3A4+CPR bactosomes), voltage-driven conversion of diclofenac to 4-hydroxydiclofenac in the presence of oxygen was examined at an applied potential of –0.6 V vs. Ag/AgCl reference (1 M KCl, CH Instruments) in 2 mL of phosphate buffer (pH 7.0) containing 100 µM of diclofenac in the presence of catalase (80 µL of 1 mg/mL catalase in pH 7.0 buffer; catalase specific activity 2000–5000 U/mg solid) or with no added catalase. The formation of 4-hydroxydiclofenac product was identified by HPLC, and its m/z was confirmed by a MS as described above under Section 2.3.

2.2.7 Estimation of H_2O_2 formed with and without addition of catalase to electrolytic solutions

Quantitation of H_2O_2 formed in the 100 μM diclofenac reaction mixture after 45 min of electrolysis using Au/cysteamine or Au/cysteamine/CYP bactosomal electrodes was carried out using an established fluorescence-based horseradish peroxidase/hydroquinone assay.[44,45] In order to understand the role of H_2O_2 in the CYP catalyzed diclofenac hydroxylation in bactosomes, electrolysis was also conducted with addition of catalase to scavenge formed peroxide.

2.3. Results and Discussion

2.3.1 Bactosomal film preparation and characterization

Figure 1A shows a schematic of the electrostatically adsorbed assembly of CPR containing CYP bactosomes on a SAM of cysteamine on a Au infused quartz crystal. The formation of the cysteamine monolayer and subsequent adsorption of CYP 2C9+CPR or 3A4+CPR bactosomes was confirmed from the decrease in oscillation frequency measured using QCM (Figure 1B-C: please note that negative frequency value is plotted on the y-axis for better understanding of the net frequency change after each wash step). Using the Sauerbrey equation,38 the amount of selfassembled cysteamine layer was estimated to be 61 ± 7 ng, and that of the subsequent electrostatically adsorbed negatively charged CYP+CPR bactosomes was estimated to be 1.60 ± 0.05 (2C9+CPR) and 1.46 ± 0.06 μg (3A4+CPR) (N = 3 replicates).

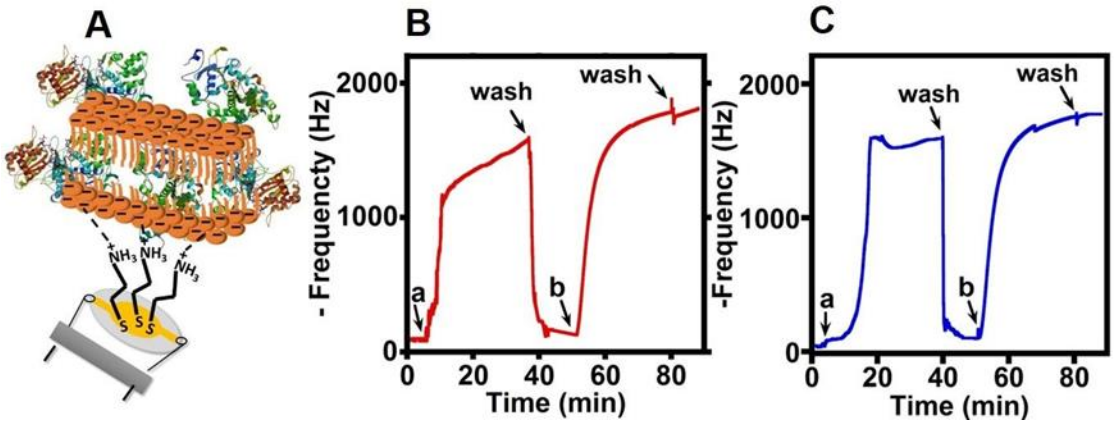

Figure 1. (**A**) Schematic of electrostatically adsorbed CYP+CPR bactosomal films on a cysteamine SAM on Au infused quartz crystals. (**B**) Real-time QCM curves showing the decrease in frequency upon the formation of the cysteamine SAM and the subsequent electrostatic adsorption of CYP 3A4+CPR bactosomes. Sample injection points: (a) 10 mM cysteamine and (b) CYP 3A4+CPR bactosomes are labeled. Similarly in (**C**), (a) is for 10 mM cysteamine and (b) is for CYP 2C9+CPR bactosomes. Once the curve reached saturating response, the crystal surface was washed in phosphate buffer (pH 7.0) to remove bulk and unbound molecules in solution. The final baseline after each wash step indicates the net frequency decrease (due to added mass) for each surface modification.

SEM images of a Au infused quartz crystal surface with a cysteamine SAM before and after the adsorption of CYP 3A4+CPR bactosomes confirmed the formation of the expected electrostatic assembly by displaying changes in surface morphologies for each step of modification (Figure S2 a–c). Faradaic impedance spectroscopy measured in a Fe(CN)63–/4– mixture (each at 1 mM concentration in the mixture) as a redox probe showed an increase in Rct of 70 Ohms for the adsorption of CYP 3A4+CPR bactosomes on the cysteamine SAM modified Au infused quartz crystal (Figure S3-A). In agreement with this finding, non-faradaic impedance measurements made in the phosphate buffer (pH 7.0) in the absence of the redox probe showed an increase in impedance of ~80 Ohms for the adsorption of the CYP 3A4+CPR bactosomal film (Figure S3-B).

2.3.2 Direct electrochemistry of CYP bactosomal films

Cyclic voltammetry was used to study the direct electron transfer properties of CYP 2C9, CPR, CYP 2C9+CPR, and CYP 3A4+CPR bactosomal films assembled on the cysteamine SAM of Au infused quartz crystals. Figure 2 shows the background subtracted CVs of these films.

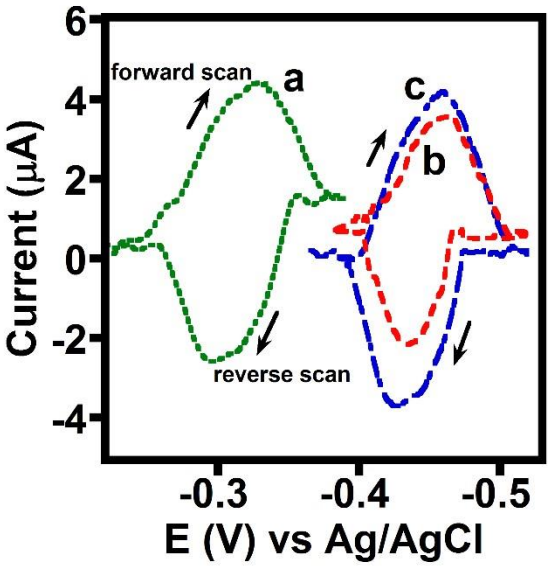

Figure 2. Background subtracted cyclic voltammograms in argon purged phosphate buffer, pH 7.0, 25 °C, scan rate 0.3 V s–1 of (a) CYP 2C9, (b) CPR, and (c) CYP 2C9+CPR bactosomal films electrostatically adsorbed on the cysteamine SAM modified Au infused quartz crystals.

The calculated formal potentials [Eo′ = (Ep, reduction + Ep, oxidation)/2; where Ep, reduction = reduction peak potential, Ep, oxidation = oxidation peak potential], electroactive surface charge (Q, area under the forward peak), and the peak width at half maximum (PWHM) of the enzyme films are detailed in Table 1. CYP 2C9 bactosomes showed a formal potential that was 140 mV more positive than the CPR containing bactosomes. The similarity in the formal potentials between the CYP, 2C9+CPR and CPR bactosomes confirms that the CPR is the electron receiver from the SAM modified Au electrode in the CYP 2C9+CPR film. The 3A4+CPR bactosomal film exhibited a reduction potential similar to that of the CPR film (Figure S4), but the reverse peak was

less prominent, probably due to lower levels of expressed CPR (by 2.5-times) compared to that of the 2C9+CPR film (Table S1, product information). Only the cysteamine SAM on the Au infused quartz crystals showed no anaerobic redox peak at this potential region. The CPR redox peaks were attributed to the FAD/FMN cofactors with the flow of electrons known in biocatalysis from

NADPH → CPR(FAD) → CPR(FMN) → CYP-heme to monooxygenate a CYP-bound substrate

to product in the presence of molecular oxygen.[9] The bactosomal CYP and CPR formal potentials are better resolved in the cysteamine SAM surface than that reported for naphthalene thiolate modified Au electrodes (−380 mV for CYP 3A4-microsomes and −410 mV for CPR-microsomes vs. Ag/AgCl).[18]

CYP 2C9+CPR showed slightly higher electroactive protein amounts than the CYP 2C9 film (Table 1). CPR bactosomes showed a slightly lower electroactive protein amount. CYP 3A4+CPR, which had half the CYP concentration and a 2.5-times lower CPR concentration, showed half the electroactive charge with respect to the CYP 2C9+CPR film. The number of electrons involved in the direct electron transfer by the bactosomal films was estimated based on the PWHM values in anaerobic CVs (Figure 2). For an ideal thin film of an adsorbed species on an electrode, the PWHM for a one electron transfer process is 90.6 mV at 25 °C.[43] The measured PWHM values shown in Table 1 suggest the non-ideal film voltammetry of the bactosomal films.

The PWHM of the CYP 2C9 bactosomal film is close to the one electron transfer process that would be expected for the CYP-heme cofactor. The PWHM of the CPR bactosomal film is close to the two electron limit and this suggests the electron receiving FAD cofactor of CPR communicating with the electrode.[17,46,47] For the CYP (2C9 or 3A4)+CPR bactosomal films, the PWHM values are lower than that of the one electron CYP 2C9 film and correspond to either the CPR FAD cofactor alone and/or an intermediate mixed electron transfer process that could involve association of CYP with the CPR as a complex in the membrane.[16] Nevertheless, the agreement

between the formal potentials of the CPR and CYP+CPR films strongly supports that CPR is the major electron receiver protein from the electrode (Table 1).

Table 1. Electrochemical properties of the films in phosphate buffer pH 7.0.

Bactosomal film type on Au/cysteamine surface	$E^{o'}$ (mV) vs. Ag/AgCl	Electroactive charge (nC)	PWHM (mV)
CYP 3A4+CPR	−440 ± 40	107 ± 12	67 ± 5
CYP 2C9+CPR	−450 ± 40	245 ± 23	62 ± 4
CYP 2C9	−310 ± 20	221 ± 19	75 ± 3
CPR	−450 ± 38	181 ± 13	56 ± 4
Control bactosomes (no CYP or CPR)	No peak	No peak	No peak
Au/cysteamine	No peak	No peak	No peak

2.3.3 Electrocatalytic oxygen reduction by CYP in bactosomal films

To examine the electrocatalytic oxygen reduction properties of CYP present in the designed bactosomal films, CV measurements were conducted in saturated oxygen buffer. Figure 3A(a–c) shows the oxygen reduction CVs of CYP 2C9, CPR, and CYP 2C9+CPR bactosomal films, respectively. Figure 3B(a–d) shows the oxygen reduction CVs of bare Au, Au/cysteamine, Au/cysteamine/control bactosomes (no CYP and no CPR), and the Au/cysteamine/CYP 3A4+CPR bactosomal film, respectively. The CYP 2C9+CPR bactosomal film provided the highest O_2 reduction current density of all films tested.

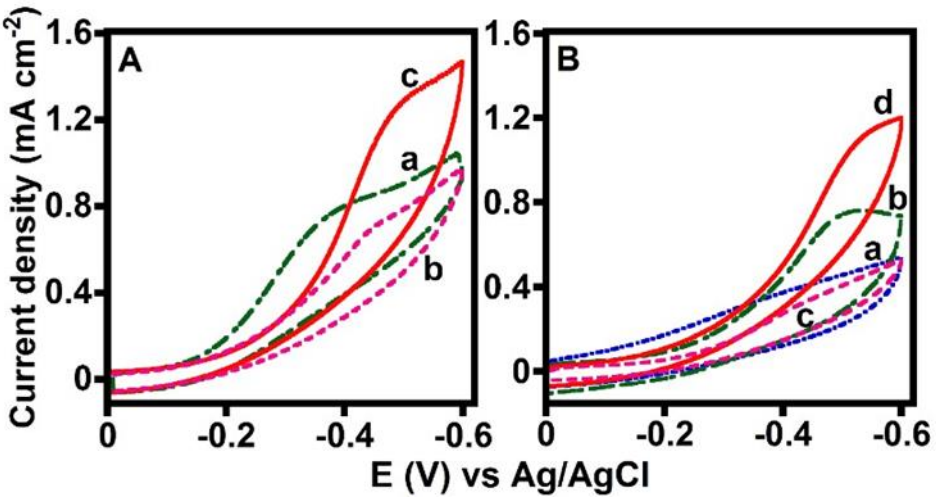

Figure 3. Catalytic oxygen reduction voltammograms of (A) (a) CYP 2C9, (b) CPR, and (c) CYP 2C9+CPR bactosomal films. (B) (a) Bare Au, (b) Au/cysteamine, (c) Au/cysteamine/control bactosomes (no CYP or CPR present), and (d) Au/cysteamine/CYP 3A4+CPR bactosomal film in a stirred solution of phosphate buffer, pH 7.0, 25 ^{O}C, under saturated oxygen conditions.

Table 2 lists the onset of O_2 reduction potentials and O_2 reduction currents measured from the catalytic CVs in Figure 3. The onset of O_2 reduction catalyzed by the CYP 2C9 bactosomal film is ~ 100 mV more positive than that of the CYP 2C9+CPR or CYP 3A4+CPR films (Table 2), which is in accordance with the formal potentials in argon for CYP-heme and CPR molecules (Figure 2). This result confirms the direct CYP 2C9 mediated electrocatalysis in the case of CYP 2C9 bactosomes. In the CYP 2C9 (or 3A4)+CPR films, the CPR mediates the transfer of electrons to CYP-heme from the electrode to initiate O_2 reduction. Furthermore, during catalysis, the CPRCYP complex formation in the CYP 2C9+CPR bactosomes likely facilitates intermolecular electron transfer from CPR to CYP-heme in a manner similar to that of the natural biocatalytic pathway.[16] The smaller O_2 reduction current catalyzed by the CYP 3A4+CPR film can be attributed to the lower amounts of CPR and CYP in this bactosomes compared to the 2C9+CPR system (Table 2 and Table S1).

Table 2. Onset of O_2 reduction potential and current densities of the bactosomal films.

Bactosomal film type on Au/cysteamine surface	Onset potential of O_2 reduction (mV)	Current density (mA cm^{-2}) at −0.5 V vs. Ag/AgCl
CYP 3A4+CPR	−235 ± 15	0.95 ± 0.09
CYP 2C9+CPR	−220 ± 11	1.30 ± 0.10
CYP 2C9	−120 ± 9.4	0.90 ± 0.10
Control bactosomes (no CYP or CPR)	−248 ± 23	0.40 ± 0.01
CPR	−224 ± 8.5	0.70 ± 0.08
Au/cysteamine	−260 ± 1.3	0.74 ± 0.03

The non-enzymatic O_2 reduction current generated by the cysteamine SAM film alone could be attributed to the secondary interactions of oxygen molecules with positively charged surface amine end groups. The resulting enrichment or localization of oxygen close to the Au surface, allows better interfacial charge transport and the oxygen reduction occurs. Similar oxygen reduction was exhibited by the CPR film with no CYP, likely arising from the electrocatalytic property of non-enzymatic cysteamine monolayer surface. However, the O_2 reduction wave shapes of the cysteamine and the CPR bactosomal films differ, probably due to differences in the interfacial double layer structures. It has been reported that small molecules such as cysteamine chemisorbed on the Au surface can exhibit electrocatalytic oxygen reduction, but the exact reason has not been determined.[48] Au and control bactosomes immobilized on the Au/cysteamine surface exhibited the smallest currents from non-enzymatic electrochemical O_2 reduction. The observed formal potentials and the onset of O_2 reduction currents indicate that (i) CYP enzyme is electrocatalytically

active in the designed bactosomal films and (ii) CPR mediates transfer of electrons to the CYP-heme in CYP (2C9 or 3A4)+CPR bactosomal films to enhance oxygen reduction.

2.3.4 Voltage-driven hydroxylation of diclofenac by bactosomal films

Voltage-driven conversion of diclofenac to 4-hydroxydiclofenac catalyzed by the designed bactosomal films (Figure 4A) was conducted at an applied potential of –0.6 V vs. Ag/AgCl for 45 min in the presence of oxygen. This negative potential (~ 150 mV more negative than the formal potential of CPR) was used to provide sufficient reducing equivalents to the CYP-heme enzyme either directly (in the case of only CYP bactosomes) or via the CPR (for CYP+CPR films).

Following electrolysis, the reaction mixture was analyzed for the hydroxylation product by HPLC. Diclofenac and 4-hydroxydiclofenac were eluted at retention times of 9 and 7.5 min, respectively (Figure 4A), which was confirmed by running diclofenac and 4-hydroxydiclofeanc standards and mass spectral identification of the expected m/z values for these compounds (Figure 4B). Two peaks with M+H values of 296 and 312 Da corresponding to the diclofenac and hydroxylated diclofenac molecules, respectively, were confirmed.

The control bactosomal film that did not contain CYP and CPR formed no hydroxylation product, and only one peak with the retention time of 9 min corresponding to the diclofenac starting compound was observed (Fig. 4A-a). Table 3 provides the turnover rates for the various CYP bactosomal films examined in this study. Based on the volume and the known concentration of CYP in bactosomes used for adsorption, we calculated the added amount of CYP in pmoles and used this value to determine the turnover rates. We used the added amount of CYP rather than the surface immobilized electroactive amount because in the case of CYP+CPR films, the electron transfer is to the CPR or its complex with CYP and not to CYP. Thus, the calculation of electroactive CYP alone from CVs is not possible. Although this could be calculated for the CYP 2C9 bactosomal film (i.e., no CPR control, Table 1), we used the added CYP amount present in the

bactosomal solutions to maintain consistency, which allowed relative comparison of turnover rates among films.

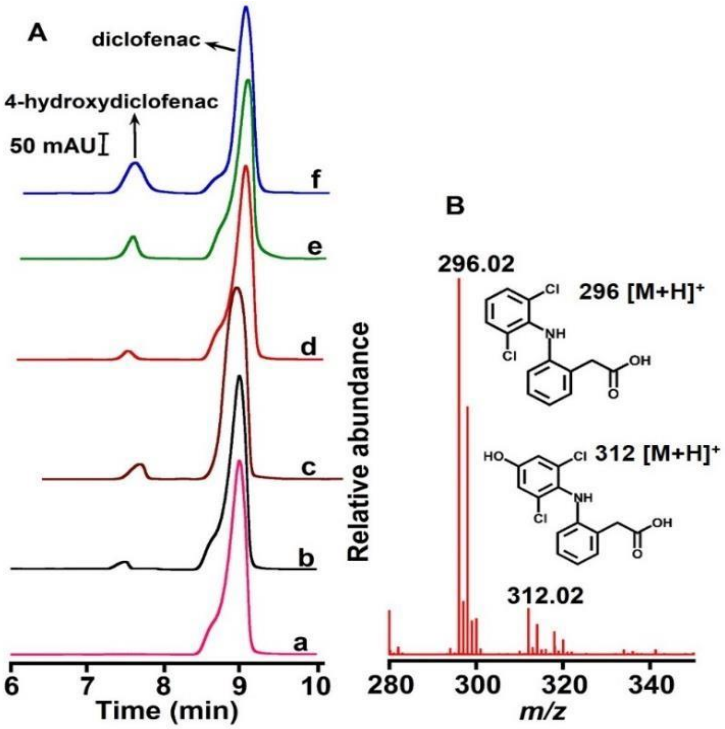

Figure 4. (A) HPLC chromatograms of reaction mixtures (100 µM diclofenac in buffer) after 45 min of applied voltage (–0.6 V vs. Ag/AgCl) to the Au/cysteamine monolayer on QCM crystals adsorbed with a film of (a) control bactosomes (no CYP or CPR present), (b) CPR, (c) CYP 3A4+CPR, (d) CYP 2C9, (e) CYP 2C9+CPR bactosomes in the absence of catalase, and (f) CYP 2C9+ CPR bactosomes in the presence of added catalase in phosphate buffer pH 7.0, saturated oxygen, 25 oC. (B) Mass spectrometry confirmation of diclofenac reactant (M+H 296 Da) and 4-hydroxydiclofenac product (M+H 312 Da) from the CYP catalyzed electrolytic reaction mixture.

Catalase was used to provide mechanistic insights about the voltage-driven biocatalysis of the bactosomal films on the SAM. The CYP 2C9+CPR bactosomal film showed a 6.5-fold (with catalase) and a 5.6-fold (without catalase) higher turnover rates than the respective CYP 2C9 bactosomal films (Table 3). The greater turnover rate for the CYP 2C9 (or 3A4)+CPR film

confirmed the role of CPR in electron transfer to CYP 2C9 from the electrode surface to facilitate CYP 2C9 catalyzed diclofenac hydroxylation in the presence of oxygen. However, the small level of product from the CPR film suggests a non-specific electrocatalytic hydroxylation of diclofenac by this film (Fig. 4A-b).

Table 3. Comparison of voltage-driven metabolite formation by different bactosomal electrodes.

Bactosomal bioelectrode	Voltage-driven CYP turnover rate (pmol roduct $pmol^{-1}$ CYP min^{-1} cm^{-2})
CYP 2C9+CPR (no catalase)	195±5
CYP 2C9+CPR (catalase)	410±22
CYP 2C9 (no catalase)	35±4
CYP 2C9 (catalase)	63±8
CYP 3A4+CPR (no catalase)	169±7
Only CPR (no catalase)	n/a
Control bactosomes (no CYP, no CPR)	n/a

2.3.5 Major CPR mediated CYP electrocatalysis in membrane-bound CYPs

In purified membrane-free soluble CYP based biocatalysis, H_2O_2 has been shown to be useful in forming the ferryloxy radical cation of CYP via the peroxide shunt pathway and facilitating substrate monooxygenation.[15] Electrochemically, H_2O_2 can be generated by dioxygen reduction under an applied negative potential catalyzed by CYP films on electrodes for subsequent use in substrate oxygenation.[49] If this was the case, then the peroxide shunt pathway of CYPs could play a role in bactosomes, as shown before for the purified CYP enzyme bioelectrodes.[49,50] The amount of H_2O_2 formed in the electrolytic reaction mixture from the Au/cysteamine/control bactosomes (containing no CYP or CPR) and Au/cysteamine/CYP 3A4+CPR bactosomal electrodes (representative film) was estimated (by the horseradish peroxidase/hydroquinone assay) to be 63.5 ± 7.7 and 75 ± 12 nmol, respectively. These H_2O_2 levels are not very different from each other, which indicates that the H_2O_2 formed is not utilized for electrocatalysis by the CYP+CPR bactosomal film and that the role of CPR in mediating electrons to reduce CYP-heme as in the natural CYP catalytic pathway is occurring (Scheme 2).

Scheme 2. CPR mediated CYP electrocatalytic pathway identified in the designed bactosomal film and the insignificance of peroxide shunt pathway in the case of membrane-bound CYP electrocatalysis.

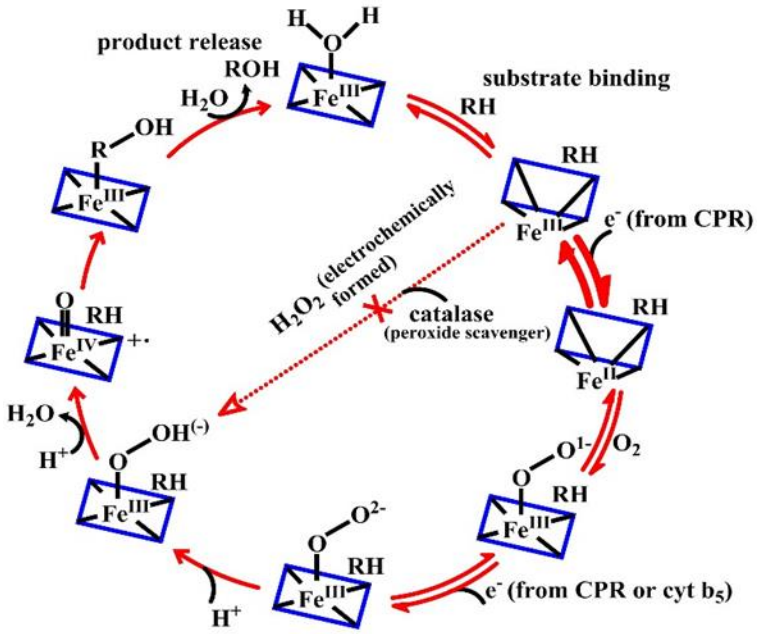

When we added an optimally identified concentration of catalase (80 µL of 1 mg/mL catalase of specific activity 2000–5000 U/mg) to the electrolysis solution containing CYP 2C9+CPR or CYP 2C9 film on a cysteamine SAM on Au quartz crystals, the added catalase was sufficient to scavenge all H2O2 formed (confirmed by the horseradish peroxidase/hydroquinone assay). This electrolytic solution was then analyzed for the absence of 4-hydroxydiclofenac product formation. In contrast to our presumption, the electrolysis reaction mixture still showed two peaks with retention times at 9 and 7.5 min for diclofenac and 4-hydroxydiclofenac, respectively, as observed for electrolysis with no added catalase (Figure 4A-d and e). In fact, addition of the catalase yielded a greater amount of hydroxylation product than when it was absent (Table 3). This observation suggests that catalase may eliminate the detrimental effect of reactive oxygen species on membranes (e.g., lipid peroxidation) from the electrochemically generated H_2O_2. As a result, the intact membrane

structure would be retained in the bactosomal film with bound CPR and CYP to offer better intermolecular electron transport from CPR to CYP and catalytic activity of CYP 2C9.

More surprisingly, the CYP 2C9 bactosomal film also formed product in the presence of added catalase. This observation suggests that for membrane-bound CYP electrocatalysis of substrate oxygenation, peroxide has no significant role. It also suggests i) complete electrochemically reduced CYP 2C9 catalysis, with a possible trace of peroxide locally utilized inside the membrane and not measurable by the peroxide assay and/or ii) residual CPR mediated CYP catalysis is possible (Table S1 for product details). Nonetheless, the combination of CYP 2C9 with CPR yielded significantly greater product than the CYP alone (Table 3). Film stability assessment by the amperometric i-t curve (applied potential −0.6 V vs Ag/AgCl) under continuous catalytic oxygen reduction for the Au/cysteamine/P450 3A4 bactosomal electrode (representative case) displayed a half-life of 4 h (Figure S5). This stability is appreciable and sufficient to conduct the electrocatalysis despite the fact that film loss and reductive desorption of thiol on Au electrodes (at –0.6 V vs. Ag/AgCl) are possible.[51]

2.4. Conclusions

This report provides new insights about the electrocatalytic pathways of CYP and CPR in a membrane environment at the molecular level for the first time. By systematically comparing CYP, CPR, and the combination of these two expressed in bactosomes, we were able to unambiguously discover the following properties: (i) in a bactosomal film, the CYP formal potential is −310 mV vs Ag/AgCl and is 140 mV more positive than that of CPR; (ii) the presence of CPR is significant for CYP electrocatalysis; (iii) H_2O_2 plays an insignificant role in the electrocatalysis of membrane-bound forms of CYP enzymes for monooxygenation of substrates; (iv) CPR mediated electrocatalysis operates in the CYP+CPR containing bactosomes; and (v) addition of catalase has

a favorable effect on enhancing the electrocatalytic product yield of CYP alone as well as CYP+CPR bactosomes. The insignificance of the H2O2 pathway in the membrane-bound form of CYP electrocatalysis contrasts with the catalysis by purified soluble forms of CYP enzymes.[10,50]

2.5 SUPPORTING INFORMATION

Table S1. Bactosomal product specifications provided by Cypex Ltd.

Product	Protein concen-tration (mg mL^{-1})	CYP concen-tration (nmol mL^{-1})	Specific CYP concen-tration (pmol mg $protein^{-1}$)	CYP Activity/V_{max} (pmol product $pmol^{-1}$ CYP min^{-1})	CPR Activity (nmol min^{-1} mg^{-1} protein)	CPR concen-tration (pmol mg $protein^{-1}$)
CYP 3A4+CPR bactosomes	10	1	100	69	574	190
CYP 2C9+CPR bactosomes	12.6	2.4	190	98	1405	470
Only CYP 2C9 bactosomes	13	2.8	215	n/a	1.1	0.4
Only CPR bactosomes	12.8	n/a	n/a	n/a	2281 nmol min^{-1} mL^{-1}	9.7 nmol mL^{-1}
Control bactosomes	10	n/a	n/a	n/a	n/a	n/a

2.5.1 Determination of total CYP 2C9 amount in bactosomes

Method

The CYP 2C9 content in 2C9+CPR bactosomes was calculated using the carbon monoxide spectral assay optimized by Cypex Ltd (Dundee, Scotland, UK; Distributor: Xenotech LLC, Kansas, USA) with slight modifications.1 Briefly, a few grains of fresh sodium dithionite were added to a ten times diluted CYP 2C9+CPR bactosomes sample (3.00 mL) and split equally into two cuvettes labeled as sample and reference. Then the two cuvettes were placed in a Cary 100 Bio UV-Visible dual beam spectrophotometer and the baseline and absorbance were recorded from 400-500 nm. Then the sample cuvette was removed from the spectrophotometer and the solution was bubbled with 5% CO at a rate of one bubble/second for 60 seconds. The sample cuvette was replaced and the overlay absorbance was recorded again from 400-500 nm. Multiple overlay scans were taken until the maximum CYP 2C9 absorbance was observed at 450 nm. The CYP 2C9 amount was calculated from the absorbance at 450 nm relative to 490 nm using the extinction coefficient of 0.091 µM-1 cm^{-1}.

Results and Calculation

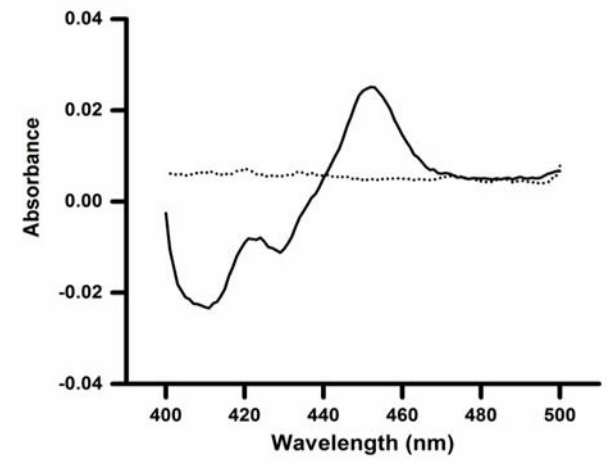

Figure S1. Difference absorption spectra of reduced CYP 2C9 bactosomes bound to carbon monoxide (solid line). Dotted line represents the base line.

Abs at 450 nm = 0.025853

Abs at 490 nm = 0.004569

Dilution factor = 10

Ɛ CYP = 0.091 µM-1 cm-1

Amount of total CYP = (OD450 - OD490)/(0.091) x Dilution

= 2.34 nmol/ml

Estimated CYP amount was comparable with the value given in the Cypex product sheet, which was 2.4 nmol/mL.

2.5.2 Determination of CYP activity of CYP 2C9+CPR bactosomes

Method

CYP activity in bactosomes was determined by the standard NADPH assay optimized by Cypex Ltd (Dundee, Scotland, UK; Distributor: Xenotech LLC, Kansas, USA). The following reagents were mixed in a 25 mL conical flask and placed in a 37° C water bath.

200 mM potassium phosphate buffer, pH 7.4 1000 µL

100 mM Magnesium chloride 250 µL

2 mM diclofenac 6.25 µL

Thawed bactosomes 6.25 µL

Water 2737.50 µL

200 mM potassium phosphate buffer, pH 7.4	1000 µL
100 mM Magnesium chloride	250 µL
2 mM diclofenac	6.25 µL
Thawed bactosomes	6.25 µL
Water	2737.50 µL

The reaction was initiated by adding 1000 µL of pre-equilibrated (at 37° C) NADPH regenerating system (5 mM NADP, 25 mM glucose-6-phosphate and 5 mM glucose-6-phosphate dehydrogenase; Xenotech LLC, Kansas, USA) to the mixture. After 10 minutes, 200 µL of the reaction mixture was withdrawn and placed in a 1.5-mL micro centrifuge tube containing 200 µL of methanol (on ice) to stop the reaction. Then the tube was centrifuged at 13,000 rpm for 10 minutes and the supernatant was analyzed by HPLC.

2.5.3 Results

The CYP 2C9 activity was determined to be 69 pmol 4-hydroxydiclofenac per pmol CYP per min for a 2.5 µM substrate concentration. This value at this diclofenac concentration was in close agreement with the CYP activity data given in the Cypex product sheet.

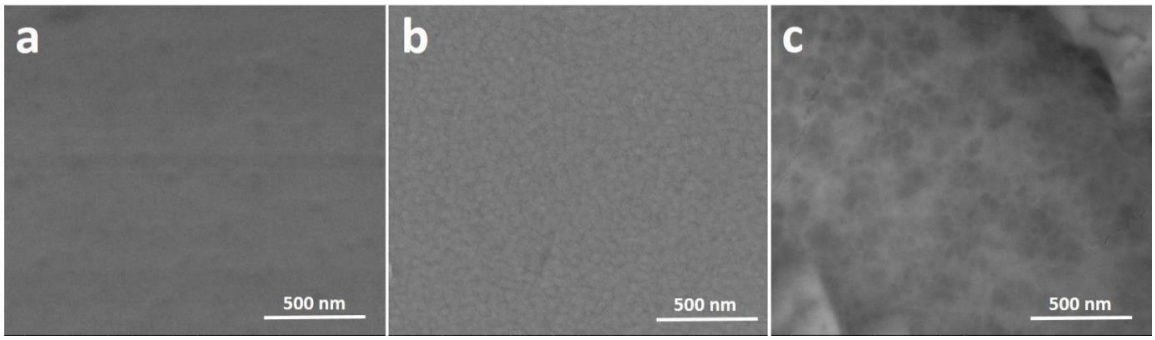

Figure S2. Representative SEM images of (a) bare Au electrode, (b) cysteamine adsorbed Au electrode, and (c) after CYP 3A4+CPR bactosome adsorption onto the cysteamine SAM.

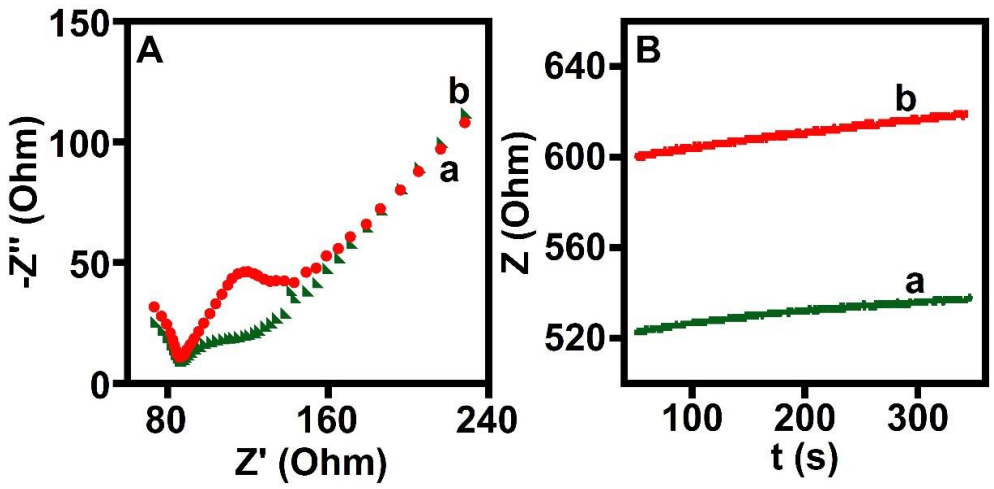

Figure S3. (A) (a) Au/cysteamine SAM and (b) after the adsorption of CYP 3A4+CPR bactosomes showing the increase in charge transfer resistance to the redox probe, Fe(CN)6 3–/4– (each at 1 mM), in phosphate buffer (pH 7.0) at 0 V vs. Ag/AgCl, and (B) the corresponding increase in non-faradaic impedance in redox probe-free phosphate buffer (pH 7.0) at 100 Hz and 0 V vs. Ag/AgCl.

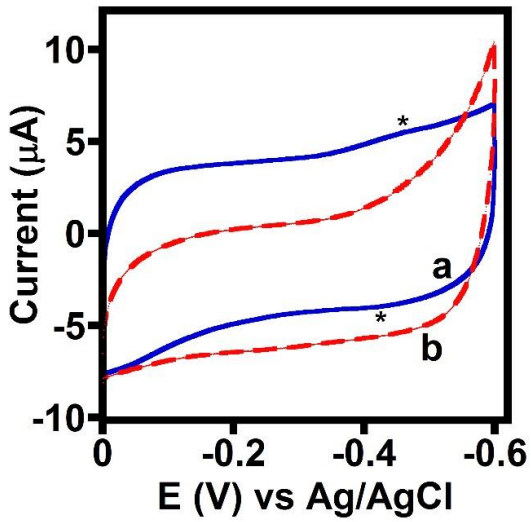

Figure S4. Cyclic voltammograms of (a) CYP 3A4+CPR bactosomes adsorbed electrostatically onto the SAM of cysteamine on a Au electrode and (b) SAM of cysteamine on a Au electrode. Scan

rate 0.3 V s^{-1}, anaerobic phosphate buffer (pH 7.0) at 25 °C (* denotes the peak positions, which are less prominent in the reverse scan due to likely lower levels of CPR than the CYP 2C9+CPR film shown in Fig. 2. So no background subtraction was attempted for this 3A4+CPR film).

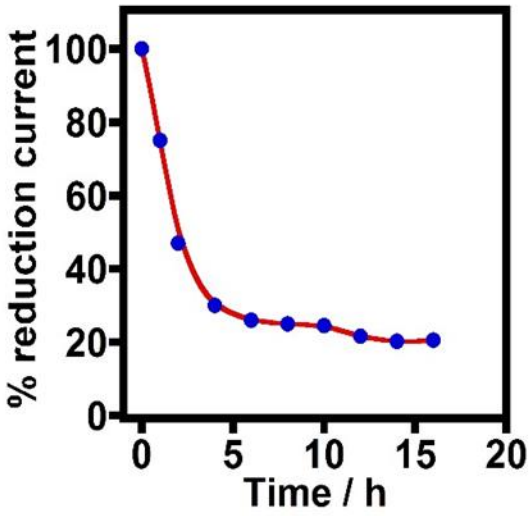

Figure S5. Amperometric i-t curve assessing the catalytic oxygen reduction stability of Au/cysteamine/CYP 3A4+CPR bactosomal electrode at an applied potential of −0.6 V vs Ag/AgCl in oxygen saturated phosphate buffer at pH 7.0 and 25 °C.

2.6 REFERENCES

1. Evans, W. E.; Relling, M. V. Science. 1999, 286, 487-491.
2. Gilardi, G.; Fantuzzi, A.; Sadeghi, S. J. Curr. Opin. Struct. Biol. 2001, 11, 491-499.
3. Krishnan, S.; Schenkman, J. B.; Rusling, J. F. J. Phys. Chem. B. 2011, 115, 8371-8380.
4. Bistolas, N.; Wollenberger, U.; Jung, C.; Scheller, F. W. Biosens. Bioelectron. 2005, 20, 2408-2423.
5. Green, M. T. Curr. Opin. Chem. Biol. 2009, 13, 84-88.
6. O'Reilly, E.; Corbett, M.; Hussain, S.; Kelly, P. P.; Richardson, D.; Flitsch, S. L.; Turner, N. J. Catal. Sci.Technol. 2013, 3, 1490-492.
7. Farwell, C. C.; Zhang, R. K.; McIntosh, J. A.; Hyster, T. K.; Arnold, F. H. ACS Cent. Sci. 2015, 1, 89-93.
8. Renata, H.; Wang, Z. J.; Kitto, R. Z.; Arnold, F. H. Catal. Sci. Technol 2014, 4, 3640-3643.
9. G. Denisov and S. G. Sligar, in Cytochrome CYP: Structure, Mechanism, and Biochemistry, ed. P. R. Ortiz de Montellano, Springer International Publishing, Cham, 2015, DOI: 10.1007/978-3-319-12108-6_3, pp. 69-109.
10. Krishnan, S.; Rusling, J. F., Electrochemically activated catalytic pathways of human metabolic cytochrome CYPs in ultrathin films. In: J. H. Zagal and F. Bedioui (eds.), Electrochemistry of N4 Macrocyclic Metal Complexes, 2nd Ed., Springer International Publishing, Switzerland, 2016, pp. 83-105, DOI: 10.1007/978-3-319-31332-0_2
11. Hagen, K. D.; Gillan, J. M.; Im, S. C.; Landefeld, S.; Mead, G.; Hiley, M.; Waskell, L. A.; Hill, M. G.; Udit, A. K. J. Inorg. Biochem. 2013, 129, 30-34.

12. Immoos, C. E.; Chou, J.; Bayachou, M.; Blair, E.; Greaves, J.; Farmer, P. J. J. Am. Chem. Soc. 2004, 126, 4934-4942.

13. Rittle, J.; Green, M. T. Science. 2010, 330, 933-937.

14. Krishnan, S.; Abeykoon, A.; Schenkman, J. B.; Rusling, J. F. J. Am. Chem. Soc. 2009, 131, 16215-16224.

15. Cirino, P. C.; Arnold, F. H. Angew. Chem. Int. Ed. 2003, 42, 3299-3301.

16. Ortiz de Montellano, P. R. Cytochrome CYP, 3rd ed.; Kluwer/Plenum: New York, 2005.

17. Sultana, N.; Schenkman, J. B.; Rusling, J. F. J. Am. Chem. Soc. 2005, 127, 13460-13461.

18. Mie, Y.; Suzuki, M.; Komatsu, Y. J. Am. Chem. Soc. 2009, 131, 6646-6647.

19. Walgama, C.; Nerimetla, R.; Materer, N. F.; Schildkraut, D.; Elman, J. F.; Krishnan, S. Anal. Chem. 2015, 87, 4712-4718.

20. Guengerich, F. P. Chem. Res. Toxicol. 2001, 14, 611-650.

21. Zhang, Z.; F. Nassar, A.-E.; Lu, Z.; B. Schenkman, J.; Rusling, J. F. J. Chem. Soc., Faraday Trans. 1997, 93, 1769-1774.

22. Udit, A. K.; Hindoyan, N.; Hill, M. G.; Arnold, F. H.; Gray, H. B. Inorg. Chem. 2005, 44, 4109-4111.

23. Shumyantseva, V. V.; Bulko, T. V.; Suprun, E. V.; Chalenko, Y. M.; Yu.Vagin, M.; Rudakov, Y. O.; Shatskaya, M. A.; Archakov, A. I. Biochim. Biophys. Acta, - Proteins and Proteomics 2011, 1814, 94-101.

24. Shumyantseva, V. V.; Ivanov, Y. D.; Bistolas, N.; Scheller, F. W.; Archakov, A. I.; Wollenberger, U. Anal. Chem. 2004, 76, 6046-6052.

25. Fantuzzi, A.; Fairhead, M.; Gilardi, G. J. Am. Chem Soc. 2004, 126, 5040-5041.

26. Fantuzzi, A.; Capria, E.; Mak, L. H.; Dodhia, V. R.; Sadeghi, S. J.; Collins, S.; Somers, G.; Huq, E.; Gilardi, G. Anal. Chem. 2010, 82, 10222-10227.

27. Shumyantseva, V. V.; Bulko, T. V.; Rudakov, Y. O.; Kuznetsova, G. P.; Samenkova, N. F.; Lisitsa, A. V.; Karuzina, I. I.; Archakov, A. I. J. Inorg. Biochem. 2007, 10, 859-865.

28. Lu, J.; Zhang, Y.; Li, H.; Yu, J.; Liu, S. Chem. Commun. 2014, 50, 13896-13899.

29. Lu, J.; Cui, D.; Li, H.; Zhang, Y.; Liu, S. Electrochim. Acta 2015, 165, 36-44.

30. Faulkner, K. M.; Shet, M. S.; Fisher, C. W.; Estabrook, R. W., Proc. Natl. Acad. Sci. USA 1995, 92, 7705-7709.

31. Estabrook, R. W.; Shet, M. S.; Fisher, C. W.; Jenkins, C. M.; Waterman, M. R., Arch. Biochem. Biophys.1996, 333, 308-315.

32. Vincent, K. A.; Parkin, A.; Armstrong, F. A. Chem. Rev. 2007, 107, 4366-4413.

33. Krishnan, S.; Rusling, J. F. Thin Iron Heme Enzyme Films on Electrodes and Nanoparticles for Biocatalysis, Chapter 5, In: New and Future Developments in Catalysis, Suib, S. L. Ed.; Elsevier Publishers, 2013, 125-147.

34. Krishnan, S.; Rusling, J. F. Electrochem. Commun. 2007, 9, 2359-2363.

35. Nerimetla, R.; Krishnan, S. Chem. Commun. 2015, 51, 11681-11684.

36. Wasalathanthri, D. P.; Malla, S.; Faria, R. C.; Rusling, J. F. Electroanalysis 2012, 24, 2049 - 2052.

37. Krishnan, S.; Wasalathanthri, D.; Zhao, L.; Schenkman, J. B.; Rusling, J. F. J. Am. Chem. Soc. 2011, 133, 1459-1465.

38. Alfonta, L.; Willner, I. Anal. Chem. 2001, 73, 5287–5295.

39. Yang, L.; Ruan, C.; Li, Y. Biosens. Bioelec. 2003, 19, 495-502.

40. Dak, P.; Ebrahimi, A.; Alam, M. A. Lab on a Chip 2014, 14, 2469-2479.

41. Singh, V.; Krishnan, S. Analyst 2014, 139, 724-728.

42. Stewart, J. C. Anal. Biochem. 1980, 104, 10-14.

43. A. Bard, L. R. Faulkner, In: Electrochemical Methods: Fundamentals and Applications, Second Ed., Wiley, NJ, USA 2001.

44. Sella, E.; Shabat, D. Org. Biomol. Chem. 2013, 11, 5074-5078.

45. Mishin, V.; Gray, J. P.; Heck, D. E.; Laskin, D. L.; Laskin, J. D. Free Radical Biol. Med. 2010, 48, 1485-1491.

46. Shukla, A.; Gillam, E. M. J.; Bernhardt, P. V. Electrochem. Commun. 2006, 8, 1845-1849.

47. Sultana, N.; Schenkman, J. B.; Rusling, J. F. Electroanalysis 2007, 19, 2499-2506.

48. Climent, V.; Fu, Y.; Chumillas, S.; Maestro, B.; Li, J.-F.; Kuzume, A.; Keller, S.; Wandlowski, T. J. Phys. Chem. C. 2014, 118, 15754-15765.

49. Zu, X.; Lu, Z.; Zhang, Z.; Schenkman, J. B.; Rusling, J. F. Langmuir 1999, 15, 7372-7377.

50. Munge, B.; Estavillo, C.; Schenkman, J. B.; Rusling, J. F. ChemBioChem 2003, 4, 82-89.

51. Zhong, C. J.; Zak, J.; Porter, M. D. J. Electroanal. Chem. 1997, 421, 9-13.

CHAPTER III

ELECTROCATALYSIS BY SUBCELLULAR LIVER FRACTIONS BOUND TO CARBON NANOSTRUCTURES FOR STEREOSELECTIVE GREEN DRUG METABOLITE SYNTHESIS

3.1 Introduction

Human liver microsomes (HLM) are subcellular fractions containing the major drug metabolizing cytochrome P450 (CYP) enzymes and their redox partner protein CYP-NADPH reductase (CPR).[1] Due to the broad range of biocatalytic reactions catalyzed by CYP enzymes (57 isoforms known in the liver) with inherent stereoselectivity, chemists have focused on the structure-function, biosensing, and catalytic applications of this unique class of enzymes.[2-7] For new drug development, HLM are being used as in vitro systems to study drug metabolism, drug inhibition, and drug-drug interactions, and to identify the specific isoforms of CYPs involved in these processes.8 These in vitro assays use NADPH as the electron source. The electrons derived from NADPH are mediated by CPR via its flavin adenine dinucleotide (FAD) and flavin mononucleotide (FMN) cofactors to reduce CYP enzymes in their heme iron-FeIII state to heme iron-Fe^{II}, which facilitates dioxygen binding. Following the second electron reduction from CPR, the strong oxidant formed (i.e., the ferryloxy-CYP cation radical) can oxygenate bound drugs.[1] Herein we describe the first liver microsomal electrocatalysis achieved on carbon nanostructure electrodes to convert a drug into its metabolite at enhanced yields.

The efficacy and pharmacokinetic properties of a drug depend on the biological activity of the metabolites formed in the liver and other organs mainly via CYP-catalyzed drug metabolism.[9] Formation of reactive metabolites from a drug can cause hepatotoxicity by damaging DNA and other cellular protein-protein interactions. Hence, it is imperative to study the physicochemical and toxicity properties of new drugs for which sufficient drug metabolites are required.[31,32] This report is significant and novel, as it demonstrates that the biocatalytic reactions of liver microsomes immobilized on high surface area nanostructure electrodes will allow the design of viable bioreactors for drug metabolite synthesis requiring only a small amount of microsomes.

Distinguished prior contributions by Arnold and co-workers include bioengineering of CYP enzymes to favorably tune the catalytic specificity and activity towards converting a desired substrate into products.[12] Rusling et al. pioneered the CYP direct electrochemistry and electrocatalysis in films of polyions and surfactants. They additionally reported layer-by-layer films of genetically engineered specific CYP with CPR or rat liver microsomes or HLM assembled with polyions for direct electrochemistry and chemical toxicity evaluations.[13] Gilardi et al. engineered CYP-fused CPR proteins to enhance catalytic activity by controlling the lifetime of the active ferryloxy oxidant form of CYP.[14] Mie et al. designed thiolated gold electrodes with hydrophobic units to immobilize supersomes and demonstrated electrocatalytic properties.[15]

Recently, our laboratory examined the influences of various carbon electrode materials in the direct electron transfer and electrocatalytic properties of immobilized HLM.[16] However, achieving highly enhanced electrocatalytic metabolite production from simple adsorption of complex HLM directly onto ‘3D’ carbon nanostructures with sufficient electrocatalytic stability and reusability features has not been reported previously. This novel, in vivo mimic biocatalytic system has the potential to realize the development of practically useful green bioreactors for

stereoselective metabolite production to assess physicochemical, toxicological, and biochemical properties of new drugs in development.

Specifically, we have discovered that HLM can be adsorbed onto multiwalled carbon nanotubes (MWNT) coated on edge plane pyrolytic graphite electrodes (EPGs) in bioactive form to offer enhanced production of drug metabolites by direct electrocatalysis. This finding simplifies the design of drug metabolizing CYP enzyme bioreactors because it eliminates the need for tedious, expensive, and time-consuming purification of CYP enzymes, and additionally allows identification of a specific liver CYP isoform involved in the metabolism of new drugs. Uniquely, we show that the designed HLM bioreactor on EPG/MWNT is reusable for metabolite generation with good stability and does not require expensive cofactors and electron transfer mediators.

3.2 Experimental

3.2.1 Chemicals and Materials

Edge plane pyrolytic graphite disk electrodes (geometric area 0.2 cm^2) were prepared from pyrolytic graphite blocks (1 in. x 1 in. x 0.5 in., Momentive Performance Ltd., Strongsville, OH) in our machine shop. Multiwalled carbon nanotubes (MWNT, purity 99.1 %) were a gift from SouthWest Nano-Technologies Inc. (SWeNT, Norman, OK). Testosterone, L-α-phosphatidylcholine (denoted as PL), and standard 6β-hydroxytestosterone were purchased from Sigma-Aldrich. Human liver microsomes (HLM, total protein: 20 mg mL^{-1}, total amount of CYP enzymes: 0.58 nmol mg-1 protein, NADPH-cytochrome c reductase activity: 171 nmol mg^{-1} protein min-1, cytochrome b5: 0.439 nmol mg^{-1} protein, cytochrome P450-NADPH reductase (CPR) concentration: 0.057 nmol mg^{-1} protein) were purchased from XenoTetch (Lenexa, KS, USA). Microsomes containing only human CPR (expressed in Escherichia coli) was purchased from

Cypex Ltd. (Dundee, Scotland, UK) [CPR concentration: 9.7 nmol mL^{-1}, total protein concentration: 12.8 mg mL^{-1}]. All other chemicals were high-purity analytical grade. Electrochemical measurements were carried out in phosphate buffer containing 0.15 M NaCl (pH 7.0) at 25 ^{O}C.

3.2.2 Instrumentation

A 3-electrode electrochemical cell consisting of an Ag/AgCl reference electrode (1M KCl, CH Instruments Inc.), a Pt wire counter electrode, and HLM adsorbed MWNT-coated PGE working electrodes were used. Electrochemical experiments were performed by using CH Instruments (Model: CHI 1040, Texas, USA). Cyclic voltammograms (CVs) were performed under argon purged anaerobic buffer to study direct electron transfer properties. For catalytic oxygen reduction studies, CVs were conducted by rotating disc voltammetry at a rotation rate of 300 rpm (EcoChemie Autolab rotator equipped with motor controller unit, Metrohm Inc., USA).[17] The surface morphology of EPG, EPG/MWNT, and HLM adsorbed EPG/MWNT electrodes were imaged by scanning electron microscopy (Model: JEOL JXM 6400).

3.2.3 Construction of MWNT modified HLM bioelectrode

Prior to use, EPG electrodes were polished on SiC paper (P320 grit), sonicated for 30 s, rinsed in deionized water and dried under nitrogen (N2). About 10 µL of MWNT (1 mg mL^{-1} dispersion in DMF, obtained by ultrasonication at room temperature for 4 h) was dry-coated on polished EPG electrodes by leaving overnight at room temperature. The MWNT coated EPG electrodes (EPG/MWNT) were then washed with deionized water and dried under N2. 20 µL of HLM was adsorbed on EPG/MWNT electrodes for 30 min at 4 °C (denoted as EPG/MWNT/HLM). The electrodes were rinsed in deionized water and stored overnight at 4 °C before conducting electrochemical and electrocatalytic measurements.

3.2.4 Electrocatalytic hydroxylation of testosterone.

The electrocatalytic conversion of testosterone to 6β-hydroxytestoserone was identified by liquid chromatography. In brief, four HLM adsorbed EPG/MWNT electrodes were placed in a 10 mL beaker containing 250 µM testosterone in 2 mL of phosphate buffer (pH 7.0). The electrolysis was carried out at an applied potential of -0.6 V vs Ag/AgCl for 1 h under saturated oxygen conditions using a multipotentiostat (CH Instruments, CHI 1040). The reaction mixture obtained from electrolysis was analyzed using high performance liquid chromatography (HPLC, premier C18 column, length 10 cm, Shimadzu). The mobile phase (30% acetonitrile, 70% water) was delivered at a flow rate 0.3 mL min^{-1}. Testosterone and 6β-hydroxytestosterone were identified based on chromatograms of standards (Sigma) run under similar conditions.

3.2.5 Hydrogen peroxide (H2O2) assay.

Hydrogen peroxide strips (EMD Millipore MQuant peroxide test strips, Billerica, MA, USA) were used to identify the H_2O_2 formation after the bulk electrolysis of testosterone hydroxylation by EPG/MWNT/HLM electrodes. The H_2O_2 formation arises from the electrocatalytic oxygen reduction by microsomal heme proteins. The electrolysis was carried out as described above. The H_2O_2 detecting strip was placed in 1 mL of 50 % diluted reaction mixture in buffer and the resulting color of the strip was compared with the H_2O_2 concentration scale provided by the manufacturer to identify the peroxide concentration formed in the electrolysis.

3.3 Results and discussion

The surface morphologies of EPGs, EPG/MWNT electrodes, and HLM-coated EPG/MWNT electrodes were characterized by scanning electron microscopy (SEM, Figure 1). The characteristic surface defects of EPGs were covered by the MWNT, and subsequent physical adsorption of HLM led to the formation of a newly coated layer around the MWNT. This finding confirmed the immobilization of HLM on the EPG/MWNT surface (Figures 1 A-C).

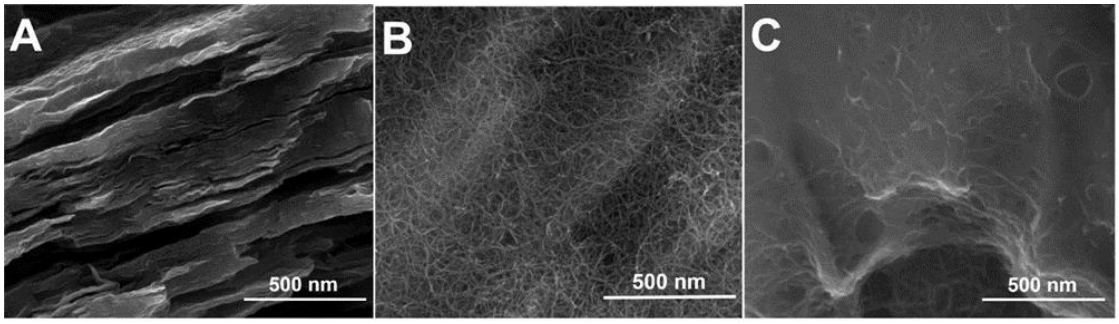

Figure 1. Representative SEM images of A. polished bar EPG electrode, B. coated MWNT on the EPG electrode, and C. HLM adsorbed onto the MWNT-modified EPG electrode.

The cyclic voltammograms of the HLM adsorbed onto EPG/MWNT electrodes displayed a redox pair at a formal potential of –0.46 V vs. Ag/AgCl (Figure 2), which is in agreement with the formal potential of microsomal CPR film alone adsorbed on similar electrodes (Figure S1) and with results of other studies.[13,18] No redox peaks at this potential region were observed for controle (Figure S2a,b). Thus, the cyclic voltammetry results confirmed the existence of direct electronic communication between HLM and MWNT-modified electrodes. Electrodes of EPG adsorbed with a phospholipid (PL) layer or EPG/MWNT in the absence of HLM (Figure S2a,b). Thus, the cyclic voltammetry results confirmed the existence of direct electronic communication between HLM and MWNT-modified electrodes.

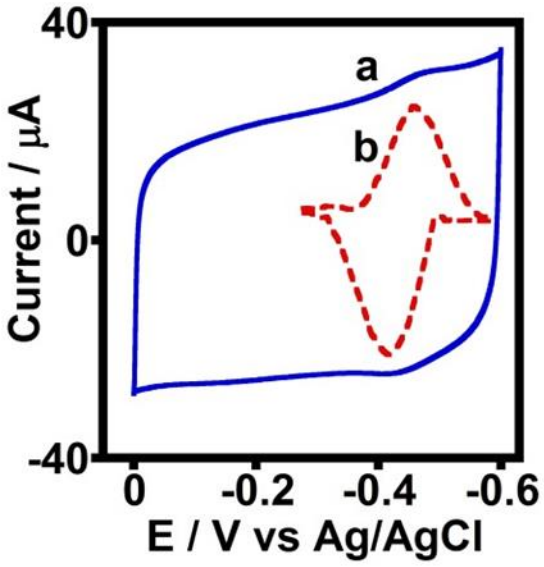

Figure 2. Cyclic voltammograms of (a) unsubtracted and (b) background subtracted EPG/MWNT/HLM electrodes in argon atmosphere, phosphate buffer (pH 7.0) at 25 ^{o}C, scan rate 0.3 V s-1.

Figure S3 shows the cyclic voltammogram of a HLM film directly adsorbed onto a EPG in the absence of MWNT. The electroactive charge was calculated to be 340 ± 30 nC for microsomal proteins on EPG/MWNT/HLM electrodes, which was comparable to that observed for EPG/HLM films in the absence of coated MWNT (400 ± 45 nC). In contrast, the electrocatalytic oxygen reduction currents catalyzed by the microsomal heme proteins on EGP/MWNT/HLM electrodes was about two times greater than that of the EPG/HLM film (Figure 3a,b). Control EPG/PL and EPG/MWNT electrodes in the absence of adsorbed HLM showed small reduction currents arising from the electrocatalytic property of the edge planes of pyrolytic graphite and those present in MWNT (Figure 3c,d).[19]

The electroactive coverage infers that compared to the enhancement factor in catalytic currents for the EPG/MWNT/HLM over the EPG/HLM electrodes, the direct electron transfer (ET) currents are not proportionately increased in EPG/MWNT/HLM. This could be due to the larger capacitive currents of MWNT-modified electrodes compared to bare EPGs (Figure

S2), which could act as a barrier to observing unhindered non-turnover currents from the EPG/MWNT/HLM electrodes in argon atmosphere. This finding also emphasizes the high enzyme turnover rates in the presence of a substrate, and it shows that the associated large catalytic currents can overcome the charging current effect of MWNT-coated electrodes (Figure 3a). In addition to the enhanced oxygen reduction currents, the EPG/MWNT/HLM electrodes exhibited greater electrode-driven bioactivity in converting testosterone to 6β- hydroxytestosterone, which is a characteristic of CYP enzymes present in HLM as explained below.

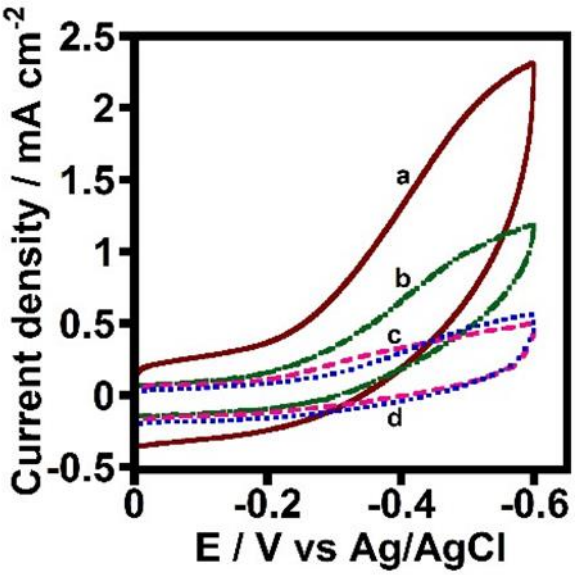

Figure 3. Rotating disc catalytic oxygen reduction voltammograms of (a) EPG/MWNT/HLM, (b) EPG/HLM, (c) EPG/MWNT, and (d) EPG/PL films in saturated oxygen, phosphate buffer (pH 7.0) at 25 °C, 300 rpm rotation rate, scan rate 0.3 V s^{-1}.

The biocatalytic properties of microsomal enzymes on EPG/MWNT/HLM and EPG/HLM electrodes were studied by bulk electrolysis at an applied potential of –0.6 V vs. Ag/AgCl in the presence of oxygen in phosphate buffer (pH 7.0) containing dissolved testosterone (250 μM). The reaction mixture was analyzed by high performance liquid chromatography. The identification of the reactant and product in the chromatograms was accomplished by running standard solutions of

testosterone and 6β-hydroxytestosterone under similar conditions (Figure S4). CYP 2C19, 2C9, and 3A4 present in HLM have been shown to hydroxylate testosterone.[20]

Figure 4 shows the chromatograms of 6β-hydroxytestosterone product formation from testosterone conversion electrocatalyzed by EPG/MWNT/HLM (chromatogram a) and EPG/HLM electrodes (chromatogram e). The absence of product formation by the control EPG/PL and EPG/MWNT electrodes (Figure S5) clearly confirms the role of CYP enzymes present in HLM in catalyzing testosterone conversion in the EPG/MWNT/HLM and EPG/HLM electrodes. The reusability of EPG/MWNT/HLM electrodes was examined by replenishing fresh testosterone solutions following each electrolysis and by repeating the reaction under an applied potential of –0.6 V vs. Ag/AgCl (chromatograms b-d).

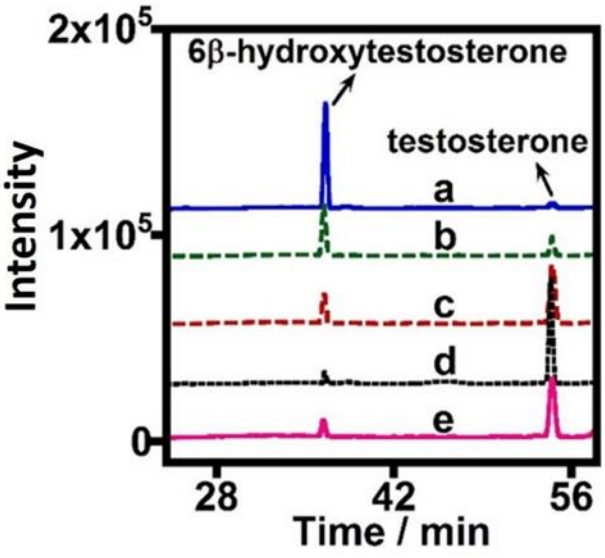

Figure 4. HPLC chromatograms of 250 µM testosterone in phosphate buffer (pH 7.0) after every 1 h bulk electrolysis of (a-d) EPG/MWNT/HLM electrodes or (e) EPG/HLM electrodes at –0.6 V vs. Ag/AgCl under saturated oxygen conditon at 25 °C. For b-d, fresh testosterone solution was supplied following the removal of each prior electrolysis reaction mixture to examine the reusability of EPG/MWNT/HLM electrodes.

Figure 5A shows the increase in currents with increasing testosterone concentration monitored by chronoamperometry at an applied constant potential of –0.6 V vs. Ag/AgCl under atmospheric air condition at 25 °C for EPG/MWNT/HLM and EPG/HLM electrodes (a and b, respectively). Control electrodes of only EPG/MWNT and EPG/PL in the absence of HLM did not show any increase in currents as shown in Figure 5A (c and d) suggesting the role of HLM in testosterone catalytic currents. We found that the large background currents under saturated oxygen condition interfered with the detection of current signals from added testosterone electrolysis in chronoamperometry. Hence, the use of atmospheric air (~ 21 % oxygen) was identified to offer small, but constant baseline currents and allowed monitoring subsequent increases in currents with testosterone concentration (Figure 5A). Electrochemical Michaelis-Menten fitting of the testosterone catalytic currents offered apparent Michaelis-Menten affinity constants (K_M^{app}) of 290 ± 33 µM for EPG/MWNT/HLM and 480 ± 51 µM EPG/HLM electrodes towards testerone substrate (Figure 5B a and b).[13a] The lower K_M^{app} of EPG/MWNT/HLM indicates the stronger affinity of HLM adsorbed to MWNT for testosterone.

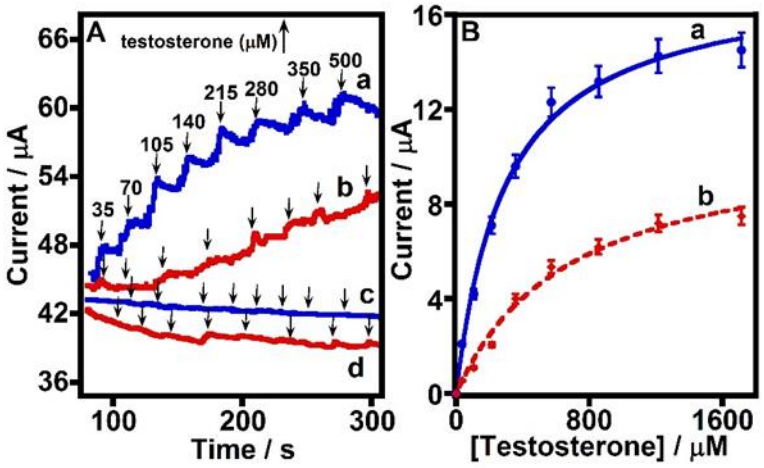

Figure 5. (A) Amperometric evidence of testosterone electrocatalysis by (a) EPG/MWNT/HLM and (b) EPG/HLM films at –0.6 V vs. Ag/AgCl, 25 °C, pH 7.0 buffer, 150 rpm electrode rotation

rate, atmospheric air condition. Amperometric curves for control electrodes (c) EPG/MWNT and (d) EPG/PL in the absence of HLM under similar conditions. (B) Electrochemical Michaelis-Menten kinetics of testosterone hydroxylation by (a) EPG/MWNT/HLM and (b) EPG/HLM films.

Results suggest that the testosterone hydroxylation by microsomal CYP enzymes in HLM may involve electron mediation by reductases from the electrode to CYPs heme centers.13,15 By obtaining the calibration plot of standard 6β-hydroxytestosterone (Figure S6), we were able to determine that 2.2 ± 0.3 and 0.45 ± 0.06 nmol of metabolite were formed by the EPG/MWNT/HLM and EPG/HLM electrodes, respectively, per unit EPG geometric area (in cm2). This suggests a 5-fold enhancement in the amount of metabolite produced by HLM immobilized on MWNT-modified electrodes. Figure 4(b) shows that 45–50 % of the initial product yield was obtained upon reuse of the EPG/MWNT/HLM electrodes. Subsequent reuses of the electrodes decreased the amount of metabolite formation to 20–25% [2nd reuse, Figure 4(c)] and 10% [3rd reuse, Figure 4(d)]. Each reaction was carried out twice for duplicate measurements, and the reproducibility of product levels was good (standard deviation was within 15%).

Figure 6 presents the film stability of HLM coated on the catalytically superior EPG/MWNT electrode in the presence of oxygen examined by chronoamperometry at an applied potential of – 0.6 V vs. Ag/AgCl in phosphate buffer (pH 7.0). The half-life of the EPG/MWNT/HLM electrode was found to be 10 h. Thus, the stability of the HLM film on EPG/MWNT electrodes did not appear to affect the catalytic yields significantly with the number of reuses. This is because within 4 h, i.e., the time sufficient to complete the biocatalysis with the reuse of electrodes for three times (Figure 4), only about 20% loss in catalytic current was noted (Figure 6).

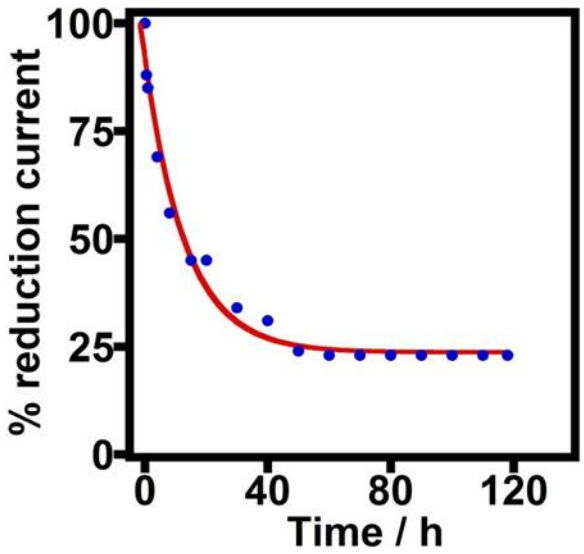

Figure 6. Amperometric i-t curve assessing the catalytic oxygen reduction stability of EPG/MWNT/HLM electrodes at an applied potential of -0.6 V vs Ag/AgCl in oxygen saturated phosphate buffer, pH 7.0 at 25 ^{o}C.

Using peroxide assay strips (Millipore Inc., MA, USA), we found that ~ 3 µmol of H_2O_2 were formed in the electrolytic reaction after 1 h electrolysis of EPG/MWNT/HLM electrodes in the presence of oxygen and testosterone. On the other hand, no detectable H_2O_2 amount was formed in the absence of HLM on EPG/MWNT electrodes under similar electrolysis conditions, suggesting the catalytic role of microsomal heme proteins in forming colorimetrically measurable peroxide levels from oxygen reduction (Figure 3).[13] We suggest the possible role of H_2O_2 towards microsomal lipid peroxidation that could cause a detrimental effect on the organization of membrane-bound microsomal enzyme films and associated electrocatalytic bioactivity.[21,22] Thus, the observed decrease in product yield with number of reuses of the EPG/MWNT/HLM electrodes was likely due to the extensive lipid peroxidation by repeated H_2O_2 stress caused by the electrolysis process. Detailed investigation is required to understand this presumed possibility.

Designing stable electrocatalytic enzyme films is a huge challenge, and we expected that doing so using complex liver microsomes on nanostructure electrodes would be even more challenging. Despite this presumption, we observed reasonably good stability for HLM films on EPG/MWNT electrodes. This suggests the favorable secondary interactions of microsomal membranes with predominantly hydrophobic MWNT to retain the intact membrane-bound protein structures with drug metabolizing bioactivity as uniquely demonstrated in this report. The favorable interaction of phospholipid membranes of HLM with MWNT appears to be also reflected in the lower K_{Mapp} of EPG/MWNT/HLM for testosterone substrate.

3.4 Conclusions

We have successfully developed a novel electrochemical liver microsomal bioreactor on carbon nanostructured electrodes for the first time. The results above suggest that the system offers direct bioelectronic communication between the microsomal proteins and '3D' MWNT modified electrodes. Electrocatalytic conversion of testosterone into its metabolite in the presence of oxygen showed significant enhancement on EPG/MWNT/HLM in comparison with EPG/HLM. The stability of the constructed bioelectrode was sufficient for reusability. Furthermore, chronoamperometry studies showed the EPG/MWNT/HLM electrode displayed high enzyme activity and strong affinity towards substrate. Our approach provides a new direction in the design of practically viable enzyme bioreactors that do not require purified enzymes and that can be used for green chemical synthesis and biosensing applications.

3.5 SUPPORTING INFORMATION

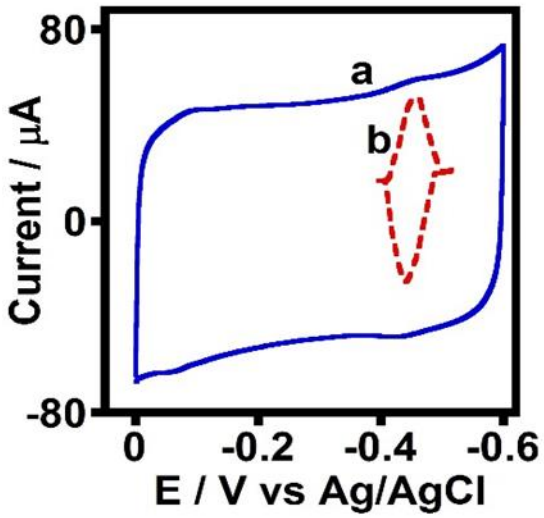

Figure S1. Cyclic voltammograms of (a) unsubtracted and (b) background subtracted EPG/MWNT/CPR electrode in argon atmosphere, phosphate buffer (pH 7.0) at 25 °C, scan rate 0.3 V s^{-1}.

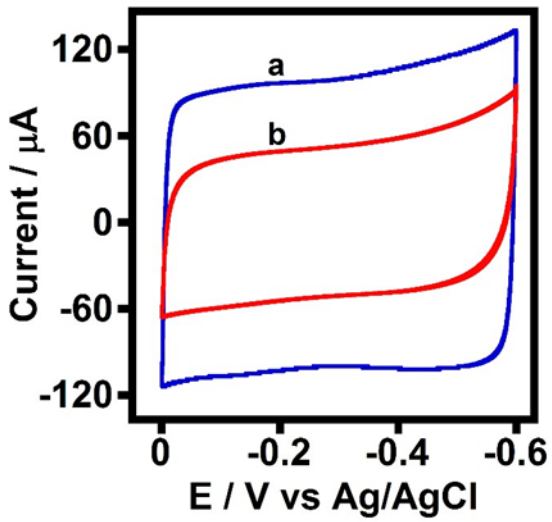

Figure S2. Cyclic voltammograms of (a) EPG/MWNT and (b) EPG/PL electrodes in the absence of HLM in argon atmosphere, phosphate buffer (pH 7.0) at 25 °C; scan rate 0.3 V s^{-1}.

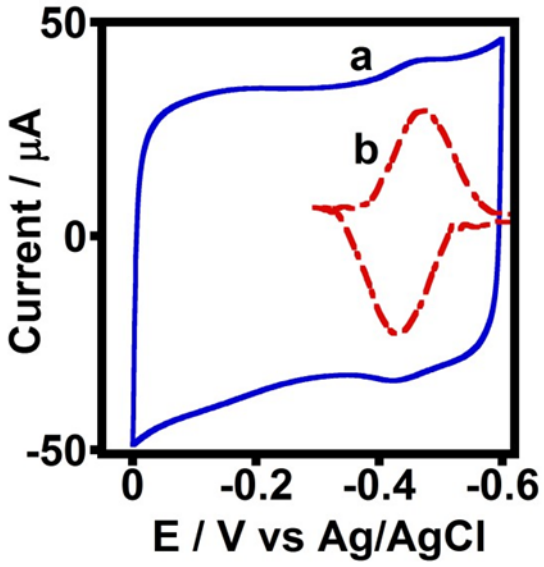

Figure S3. Cyclic voltammograms of (a) unsubtracted and (b) background subtracted EPG/HLM electrode in argon atmosphere, phosphate buffer pH 7.0 at 25 ^{O}C, scan rate 0.3 V s^{-1}.

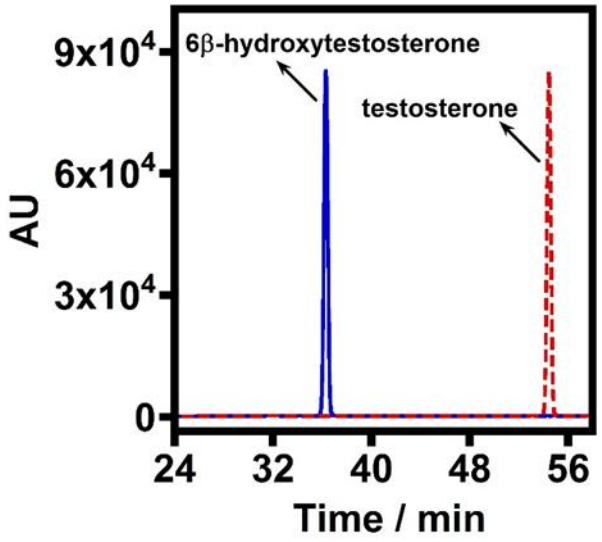

Figure S4. High performance liquid chromatograms of 250 μM testosterone and 6β-hydroxytestosterone standards in phosphate buffer (pH 7.0) at 25 °C.

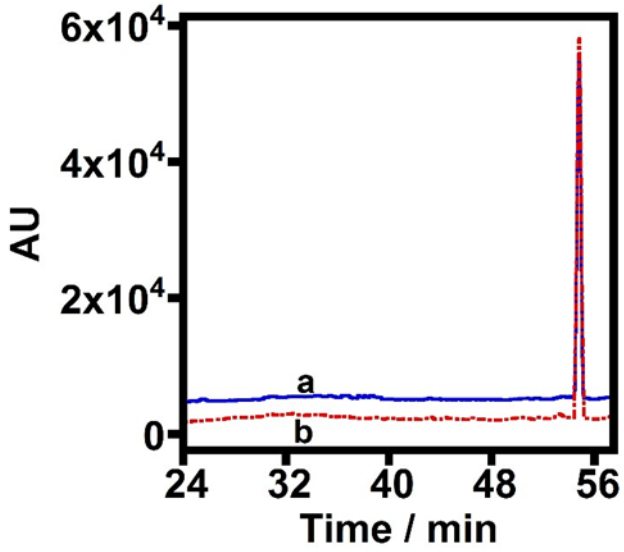

Figure S5. High performance liquid chromatograms of reaction mixtures after 1 h bulk electrolysis of (a) EPG/MWNT and (b) EPG/PL electrodes (no HLM present) in 250 μM testosterone, phosphate buffer pH 7.0 at -0.6 V vs Ag/AgCl under saturated oxygen conditions at 25 °C.

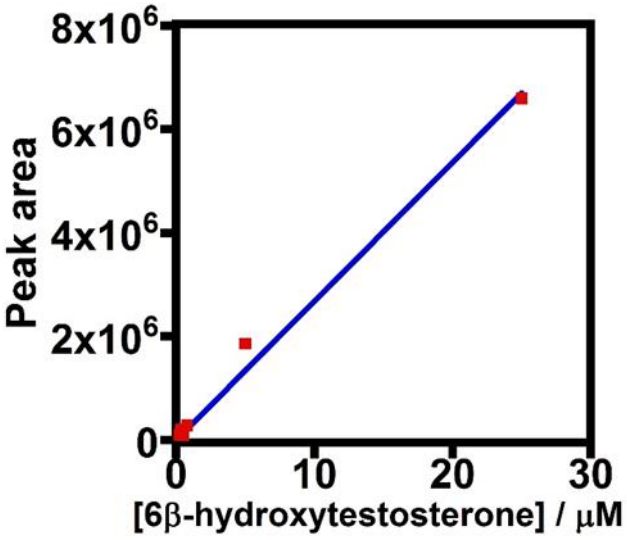

Figure S6. Calibration plot showing the peak area versus concentration of standard 6β-hydroxytestosterone.

3.6 REFERENCES

1. Ortiz de Montellano, P. R. 3rd Ed., Cytochrome P450, Kluwer/Plenum, New York, 2005.
2. (a) Guengerich, F. P.; Munro, A. W. J. Biol. Chem. 2013, 288, 17065-17073; (b) Guengerich, F. P. J. Biochem. Mol. Toxicol. 2007, 21,163-168
3. Zanger, U. M.; Schwab, M. Pharmacol. Ther. 2013, 138, 103-41.
4. Li, A. P. Drug Discov. Today Technol. 2005, 2, 179-185.
5. (a) Krishnan, S.; Bajrami, B.; Hvastkovs, E. G.; Choudhary, D.; Schenkman, J. B.; Rusling, J. F. Anal. Chem. 2008, 80, 5279-5285; (b) Wasalathanthri, D. P.; Li, D.; Song, D.; Zheng, Z.; Choudhary, D.; Jansson, I.; Lu, X.; Schenkman, J. B.; Rusling, J. F. Chem. Sci. 2015, 6, 2457-2468.
6. Schneider, E.; Clark, D. S. Cytochrome P450 (CYP) enzymes and the development of CYP biosensors, Biosens. Bioelec. 2013, 39, 1-13.
7. O'Reilly, E.; Koehler, V.; Flitsch, S.; Turner, N. Chem. Commun. 2011, 47, 2490-2501.
8. Wienkers, L. C.; Heath, T. G. Nat. Rev. Drug Discov. 2005, 4, 825-833.
9. Ma, Q.; Lu, A. Y. H. Pharmacol. Rev. 2011, 63, 437-459.
10. Park, B. K.; Boobis, A.; Clarke, S. et al. Nat. Rev. Drug Discov. 2011, 10, 292-306.
11. Deavall, D. G.; Martin, E. A.; Horner, J. M.; Roberts, R. J. Toxicol. vol. 2012, Article ID 645460, 13 pages, 2012. doi:10.1155/2012/645460
12. Jung, S. T.; Lauchli, R.; Arnold, F. H. Curr. Opin. Biotechnol. 2011, 22, 809-817.
13. (a) Krishnan, S.; Schenkman, J. B.; Rusling, J. F. J. Phys. Chem. B 2011, 115, 8371-8380; (b) Krishnan, S.; Wasalathanthri, D.; Zhao, L.; Schenkman, J. B.; Rusling, J. F. J. Am. Chem. Soc. 2011, 133, 1459–1465; (c) Sultana, N.; Schenkman, J. B.; Rusling, J. F.

Electroanalysis 2007, 19, 2499-2506.

14. Dodhia, V. R.; Sassone, C.; Fantuzzi, A.; Nardo, G. D.; Sadeghi, S. J.; Gilardi, G. Electrochem. Commun. 2008, 10, 1744-1747.

15. Mie, Y.; Suzuki, M.; Komatsu, Y. J. Am. Chem. Soc. 2009, 131, 6646-6647.

16. Walgama, C.; Nerimetla, R.; Materer, N. F.; Schildkraut, D.; Elman, J. F.; Krishnan, S. Anal. Chem. 2015, 87, 4712-4718.

17. (a) Krishnan, S.; Abeykoon, A.; Schenkman, J. B. Rusling, J. F. J. Am. Chem. Soc. 2009, 131, 16215-16224; (b) Krishnan, S.; Armstrong, F. A. Chem. Sci. 2012, 3, 1015-1023.

18. Shukla, A.; Gillam, E. M. J.; Bernhardt, P. V. Electrochem. Commun. 2006, 8, 1845-1849.

19. Banks, C. E.; Compton, R. G. Analyst 2006, 131, 15-21.

20. Yamazaki, H.; Shimada, T. Arch. Biochem. Biophys. 1997, 346, 161-169.

21. Ursini, F.; Maiorino, M.; Ferri, L.;Valente, M.; Gregolin, C. J. Inorg. Biochem. 1981, 15, 163-169.

22. Iqbal, M.;Okazaki, Y.; and Okada, S. Teratog. Carcinog. Mutagen. 2003, 23, 151–160.

CHAPTER IV

CORRRELATING THE ELECTROCHEMICAL KINETICS OF MYOGLOBIN-FILMS TO pH DEPENDENT MEAT COLOR

4.1 Introduction

The color of meat is the first deciding factor that influences the purchase decisions of consumers.[1] Meat color is primarily determined by the oxidation state of myoglobin (Mb).[2,3] For example, the red color of meat is influenced by the proportion of oxymyoglobin (Mb-FeII-O2) to metmyoglobin (Mb-FeIII) present. The greater the Mb-FeII-O2/Mb-FeIII ratio the brighter the red color. Mb has been a good electrochemical model heme-protein due to its easy commercial availability, relatively inexpensive nature, and peroxidase-like enzyme activity. Several electrochemical studies were reported on the direct electron transfer (ET) and catalytic peroxidase-like reduction kinetics of Mb films constructed on electrodes.[4 -7] In addition, the role of distal histidine (His-64) in the direct electron transfer properties and oxygenation of myoglobin were well documented.[8 -14] Recently, the application of nanomaterials in enhancing the redox and catalytic properties of Mb and other heme enzymes were also examined.[15 -19] Moreover, Mb-modified electrodes were designed to provide sensitive peroxide detection and other sensing and certain catalytic applications.[7,20 -22] The redox potential of Mb in meat changes with pH. In an electrochemical sense, one can observe that the electron-transfer process in a heme-protein is coupled with proton transfers, from the more positive formal potential shifts with decreasing pH, as per the Nernst equation.[10,13] Numerous research reports are available on the proton-coupled electron-transfer processes in myoglobin and its oxygen-reduction properties.[4,10,13,54-56]

However, to our knowledge, understanding the color of meat with respect to pH conditions, from the electrochemical kinetics of metmyoglobin reduction rate and oxymyoglobin formation-constant, has not been reported before.

4.2 Experimental

Equine heart myoglobin (Mb), monosodium dihydrogen phosphate, disodium hydrogen phosphate, and sodium chloride were purchased from Sigma. High-purity graphite-disk (HPG, EDM Inc., MN, USA) electrodes were used for both cyclic voltammetry (CV) and rotating disk electrochemistry (RDE). For RDE experiments, an electrode rotation rate of 2000 rpm (Eco Chemie Autolab rotator with a motor controller, Metrohm Inc., USA) was employed. Electrochemical measurements were performed in a 3-electrode electrochemical cell (CH instruments, Model CHI 6017, Texas, USA) employing a Ag/AgCl reference electrode (1 M KCl, CH Instruments), a Pt-wire counter electrode, and HPG rotating disk working electrode coated with a Mb film. Before use, HPG-electrodes were polished on P320 SiC-grit paper, rinsed well in water, and dried under nitrogen.

The myoglobin films on electrodes were prepared by placing a solution of myoglobin (3 mg mL^{-1} in the respective pH-buffer) for 10 min on freshly polished HPG-electrodes at 4 °C to allow physisorption involving electrostatic and other secondary interactions of Mb with the electrode surface.10 The free Mb solution was rinsed off in deionized water and the Mb-film coated electrodes were then used for electrochemical measurements. CV was performed under nitrogen atmosphere at different pH conditions to obtain reduction and oxidation peak potentials with increasing scan rate, and to determine the rates of metmyoglobin, Mb-Fe^{III}, reduction rate, and its reoxidation in the reverse scan. RDE was conducted at different concentrations of oxygen in nitrogen, added to the cell using 2 mass flow controllers (Aalborg Instruments & Controls Inc.,

NY, USA).[26] To investigate the oxymyoglobin formation constant at pH 5.6, 6.4 and 7.4, electrochemical Michaelis-Menten kinetics were employed. Unless otherwise specified, mixed sodium phosphate buffer solutions were used (0.1 M containing 0.15 M NaCl, pH 5.6, pH 6.4, or pH 7.4) to make Mb solutions in each pH buffer, to prepare the respective films on polished HPG electrodes, and to do the electrochemical experiments in the respective Mb-free pH buffer.

4.3 Results and discussion

Immediately after harvesting an animal, the postmortem metabolism changes from aerobic to anaerobic. This shift in metabolism results in the accumulation of lactic acid as an end product, hence, the pH drops from 7.4 (physiological pH) to 5.6 (postmortem muscle pH).[27] On the other hand, animals exposed to chronic stress such as that arising from transportation and temperature, before being slaughtered, leads to the production of certain levels of glycogen in the tissue. Therefore, the pH drop is relatively less (pH 6.4) as there exists limited glycogen availability to form lactic acid. There are several factors that can affect meat color. For example, postmortem muscle is biochemically active and enzymes such as cytochrome-b5 reductase and lactate dehydrogenase can influence the meat-color by providing reducing equivalents to heme-proteins including Mb, which is a main-pigment in meat-muscle.

In addition, oxidation of lipids can generate various primary and secondary lipid-oxidation products which can accelerate myoglobin-oxidation.[28] Previous research has utilized spectrophotometric methods to characterize myoglobin oxidation and oxygenation. However, limited knowledge is currently available regarding the reduction kinetics of metMb at different pH.

Using Mb-films immobilized on high-purity graphite (HPG) electrodes, we demonstrate here the usefulness of protein-film electrochemistry in the preliminary understanding and correlation to the pH dependent meat-color.

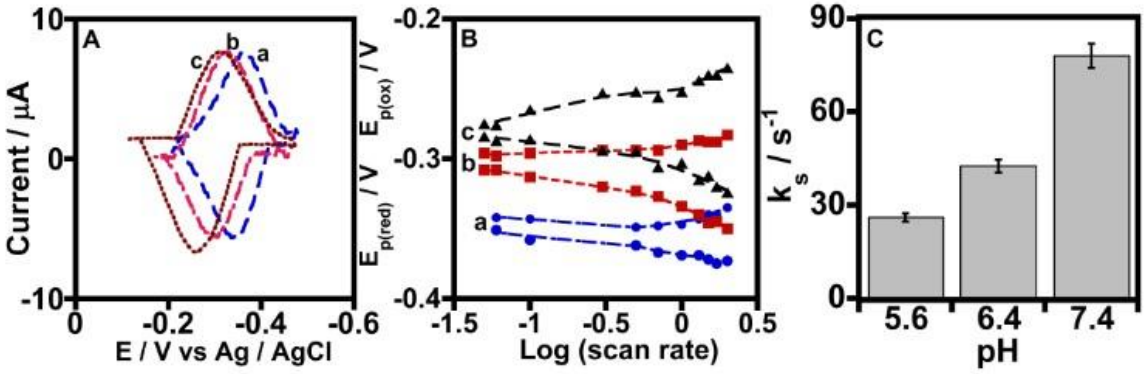

Figure 1. (A) Representative background subtracted cyclic voltammograms of Mb films adsorbed on HPG electrodes in anaerobic mixed phosphate buffers at (a) pH 7.4, (b) pH 6.4, and (c) pH 5.6. Scan rate: 0.7 Vs-1, 25oC. (B) Trumpet plots showing the peak separation with increasing scan rate for Mb-films on HPG electrodes at pH conditions defined in (A). (C) Direct electron transfer rate constants determined by Laviron's method for the Mb films at pH 7.4, 6.4 and 5.6.

In the current study, equine myoglobin was selected as the myoglobin model because it shares 88.2 and 90.8 % homology with bovine and porcine myoglobins, respectively (www.expasy.org), and it is easily obtained through commercial sources. The bioactivity of the Mb-film was tested by choosing the oxidation of o-methoxyphenol as a model reaction.[29,30] Four HPG electrodes coated with Mb-films were used to catalyze the reaction to obtain enough products for suitable measurement by absorbance. The Mb-films were found to be active in converting o-methoxyphenol (25 nmol) into 3,3'-dimethoxy-4,4'-biphenylquinone (9 nmol) in the presence of hydrogen peroxide (0.5 mM). The product formation was confirmed by measuring the absorbance maximum at 482 nm.[31]

Fig. 1A shows the representative anaerobic cyclic voltammograms of Mb-films physisorbed on HPG-electrodes at the designed three pH conditions. The peak potentials shifted more positive with decreasing pH from 7.4 to 5.6, confirming the proton-coupled ET-process. The shifts in midpoint potential per pH-unit was 56 mV (Table 1), which is close to the ideal nernstian shift of

59 mV pH^{-1} for a one-electron proton coupled ET-process.[32] The electroactive enzyme coverage was 0.02-0.03 nmol cm-2 in the pH range 5.6-7.4. Within this pH range, the reduction peak potentials shifted more negative with increasing scan rate, the peak-current versus scan rate was linear, the oxidation to reduction peak current ratios were close to unity, and the average peak-width at halfheight was around 130 mV (Table 1). All these properties suggest non-ideal surface-voltammetry of Mb-films at the tested pH values on HPG-electrodes.[13,18,19]

Fig. 1B displays the peak-separation between the oxidation and the reduction for Mb-films at different pH-values with the logarithm of scan rate (so called "trumpet plots"). The observed extent of peak-separation with pH was in the following order: pH 5.6 > pH 6.4 > pH 7.4. From the increase in peak-separation with scan rate, we obtained the direct ET-rate constants for metmyoglobin-reduction and reoxidation in the designed Mb films by Laviron's method.[33]

The rates of metmyoglobin reduction were observed to be in the following order at three different pH values [technically it is the overall rate for a quasi-reversible redox process, however, for practical convenience, we are terming it as the metmyoglobin reduction due to its propensity to complex with O2 under normal exposure to air in a meat, where Mb-reduction is performed by redox partner proteins]: pH 7.4 > pH 6.4 > pH 5.6. The smaller peak-separation observed for Mbfilms at pH 7.4 correlated well with its greater metmyoglobin reduction rate at this compared with pH 6.4 and pH 5.6 conditions (Fig. 1C).

Figures 2A-C represent the steady-state oxymyoglobin reduction currents with increasing oxygen concentration for Mb-films adsorbed on HPG-electrodes at pH 7.4, 6.4, and 5.6, respectively. The corresponding plots of oxygen concentration with the electrochemical reduction of formed Mb-FeII-O2 yielding reduction currents at each pH condition are shown in Figures 2DF, respectively. The formation constants of Mb-FeII-O2 at different pH conditions can be related to the Michaelis-Menten KM values. Here, lower KM indciates higher O2 binding affinity of Mb at

a given pH. The extent of oxymyoglobin formation decides the intensity of the bright-red color of a meat. The pH-dependent increasing order of average K_M values obtained from the MichaelisMenten fit18 of the data shown in Figures 2D-F was the following: pH 7.4 < pH 5.6 ≈ pH 6.4 (Table 1).

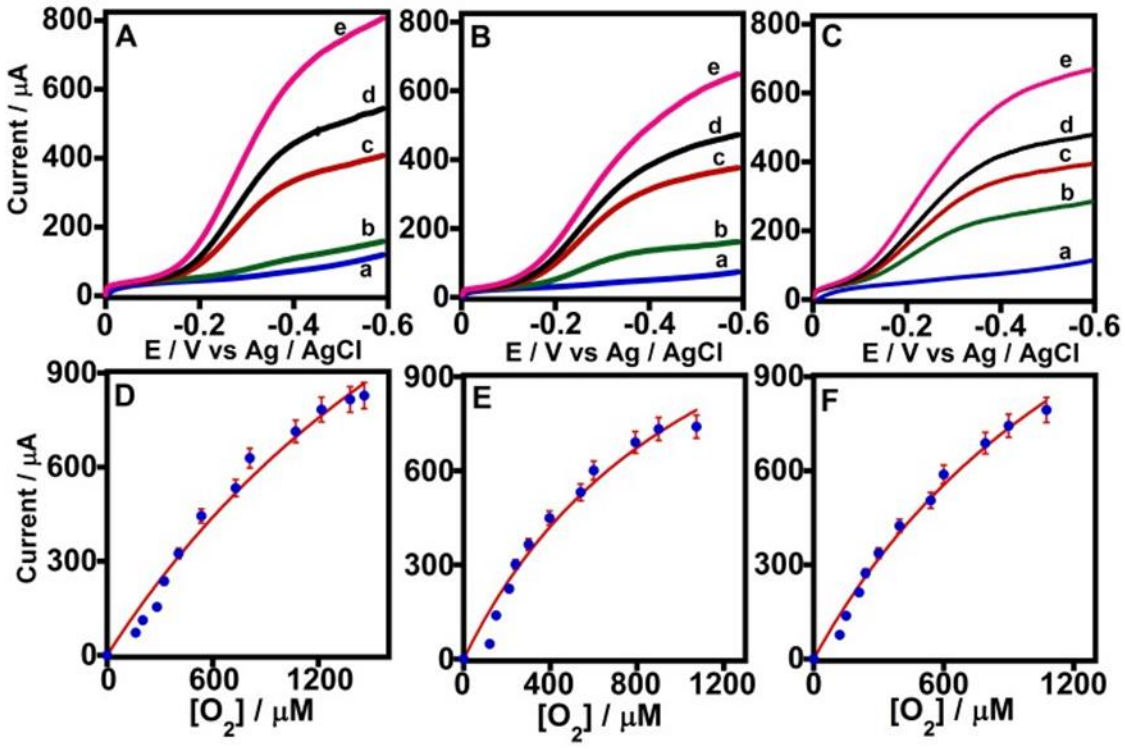

Figure 6.2. Steady-state oxymyoglobin reduction voltammograms of Mb films adsorbed on HPG electrodes with increasing oxygen concentration at (A) pH 7.4, (B) pH 6.4, and (C) pH 5.6. The oxygen concentrations shown are a. 0, b. 210, c. 300, d. 396, and e. 600 µM. The corresponding oxymyoglobin reduction currents versus oxygen concentration following the Michaelis-Menten kinetics are shown for (D) pH 7.4, (E) pH 6.4, and (F) pH 5.6. Experimental conditions: 25 ^{o}C, 2000 rpm rotation rate, scan rate 0.1 V s^{-1}.

Table 6.1. Electrochemical properties and oxymyoglobin affinity constants at pH 5.6, 6.4, and 7.4.

pH	E / V vs Ag / AgCl	Γ / (nmol cm^{-2})	Peak-width at half –height (mV)	K_M (μM)
5.6	-0.27 (± 0.01)	0.03 (± 0.01)	131 (± 10)	742 (± 90)
6.4	-0.31 (± 0.01)	0.03 (± 0.01)	127 (± 5)	780 (± 82)
7.4	-0.37 (± 0.01)	0.02 (± 0.005)	130 (± 9)	551 (± 35)

Thus, at pH 7.4, the formation of oxymyoglobin seems to be highly enhanced due to the observed high affinity between O_2 and reduced metmyolobin (low K_M, Table 1). This is additionally supported by the contribution from faster metmyoglobin reduction rate at pH 7.4 as shown in Fig. 1C. Whereas, the oxymyoglobin formation as well as the metmyoglobin reduction rates are relatively weaker at acidic pH 5.6 and pH 6.4 conditions (Fig. 1C and Table 1). This implies a large proportion of Mb-molecules present as metmyoglobin at acidic conditions, and hence the associated fading color of meat at pH 5.6 with time. While at physiological pH 7.4, both the metmyoglobin reduction rates and oxymyoglobin formation constant are significantly enhanced (Figure 1C and Table 1, K_M values), and thus can favor the red color of meat at this pH.

In agreement to prior studies, the highly possible enhanced H-bond network around distal His64 (pKa 6.0)[9] in Mb with decrasing pH from 7.4 to 5.6 is suggested to increase the activation barrier for ET.[10,13] This in turn can explain the observed decreasing order of ET-rates of metMb films from pH 7.4 to 5.6 (Fig. 1C), and the correlating trend of oxygenation affinity constant that requires the reduced-Mb-Fe^{II} state for O_2 binding (Table 1). The observed direct

elecrochemical properties are also in good correlation with the biochemical and redox-titration studies that reported the faster decoloration of meat with lowering pH conditions.[34-36] In addition, the metmyoglobin reducing activity in beef is often used as a tool to predict beef color. For example, a greater reducing activity results in brighter red meat color. Thus, our study is the first of its kind in providing insights on the color of meat with pH from the electrochemical investigation of metmyoglobin reduction and oxymyoglobin formation rates, by using an electrode as the electron donor that mimicked the in vivo function of reductases in delivering electrons to Mb.[37]

4.4 Conclusions

In summary, the results presented above demonstrate that direct electrochemistry of Mb-films can provide insights on the color of meat with pH conditions. We have tested three pH conditions, relevant to the physiological, stressed animal muscle, and post-mortem meat. The observed greater electrochemical metmyoglobin reduction rate and stronger oxymyoglobin formation constant at pH 7.4, correlated well with the bright-red color of fresh meat at this pH over acidic conditions. Thus, understanding the biochemical redox-processes of myoglobin by electrochemical methods is invaluable in designing novel tools to predict meat color and quality.

4.5 REFERENCES

1. Mancini, R. A.; Hunt, M. C., Meat Science 2005, 71, 100.
2. Livingston, D. J.; Brown, W. D., Food Technol. 1982, 35, 244–252.
3. Suman, S. P.; Joseph, P., Annu. Rev. Food Sci. Technol. 2013, 4, 79.
4. Lvov, Y. M.; Lu, Z.; Schenkman, J. B. X. Zu, J. F. Rusling, J. Am. Chem. Soc. 1998, 120, 4073.
5. Wang, S.-F.; Chen, T.; Zhang, Z.-L.; Shen, X.-C.; Lu, Z.-X.; Pang, D.-W.; Wong, K.-Y., Langmuir 2005, 21, 9260.
6. Dai, Z.; Xiao, Y.; Yu, X.; Mai, Z.; Zhao, X.; Zou, X., Biosens. Bioelec. 2009, 24, 1629.
7. Guto, P. M.; Rusling, J. F. J., Phys. Chem. B 2005, 109, 24457.
8. Olson, J. S.; Mathews, A. J.; Rohlfs, R. J.; Springer, B. A.; Egeberg, K. D.; Sligar, S. G.; Tame. J.; Renaud, J.-P.; Nagai, K. Nature 1988, 336, 265.
9. Esquerra, R. M.; Jensen, R. A.; Bhaskaran, S.; Pillsbury, M. L.; Mendoza, J. L.; B. W. Lintner, Kliger, D. S.; Goldbeck, R. A., J. Biol. Chem. 2008, 283, 14165.
10. Van Dyke, B. R.; Saltman, P.; Armstrong, F. A., J. Am. Chem. Soc. 1996, 118, 3490.
11. Svistunenko, D. A.; Sharpe, M. A.; Nicholls, P.; Blenkinsop, C.; Davies, N. A.; Dunne, J.; M. T. Wilson, Cooper, C. E., Biochem. J. 2000, 351, 595.
12. Ordway, G. A.; Garry, D. J., J. Exp. Biol. 2004, 207, 3441.
13. Nassar, A.-E. F.; Zhang, Z.; Hu, N.; Rusling, J. F., J. Phys. Chem. B 1997, 101, 2224.
14. Feng, M.; Tachikawa, H., J. Am. Chem. Soc. 2001, 123, 3013.
15. Li, Y.; Li, Y.; Yang, Y., Bioelectrochemistry 2011, 82, 112.
16. Krishnan, S.; Rusling, J. F.; Thin Iron Heme Enzyme Films on Electrodes and

Nanoparticles for Biocatalysis, in New and Future Developments in Catalysis, Chapter 5, (Ed.: S. L. Suib), Elsevier Publishers, 2013, pp. 125-147.

17. Cao, W.; Wei, C.; Hu, J.; Q. Li, Electroanalysis 2008, 20, 1925.
18. Krishnan, S.; Walgama, C., Anal. Chem. 2013, 85, 11420.
19. Walgama, C.; Krishnan, S., J. Electrochem. Soc. 2014, 161, H47.
20. Yu, X.; Chattopadhyay, D.; Galeska, I.; Papadimitrakopoulos, F.; Rusling, J. F., Electrochem. Commun. 2003, 5, 408.
21. Duan, L.-S.; Xu, Q.; Xie, F.; Wang, S.-F., Int. J. Electrochem. Sci. 2008, 3, 118.
22. Esplandiu, M. J.; Pacios, M.; Cyganek, L.; Bartroli, J.; del Valle, M., Nanotechnology 2009, 20, 355502.
23. Munge, B.; Estavillo, C.; J. B. Schenkman, J. F. Rusling, ChemBioChem 2003, 4, 82.
24. Babaei, A.; Garrett, D. J.; Downard, A. J., Int. J. Electrochem. Sci. 2012, 7, 3141.
25. Krishnan, S.; Rusling, J. F., Electrochem. Commun. 2007, 9, 2359.
26. R. Sander, Compilation of Henry's law constants for inorganic and organic species of potential importance in environmental chemistry, Version 3, 1999. Available at www.henrys-law.org
27. Scheffler, T. L.; Park, S.; Gerrard, D. E., Meat Science 2011, 89, 244–250.
28. Faustman, C.; Sun, Q; Mancini, R. A.; Suman, S. P., Meat Science 2010, 86, 86–94.
29. Doerge, D. R.; Divi, R. L.; Churchwell, M. I. Anal. Biochem. 1997, 250, 10-17.
30. Sato, H.; Hayashi, T.; Ando, T.; Hisaeda, Y.; Ueno, T.; Watanabe, Y. J. Am. Chem. Soc. 2004, 126, 436-437.
31. Guto, P. M.; Kumar, C. V.; Rusling, J. F. Langmuir 2008, 24, 10365-10370.
32. Bard, A.; Faulkner, L. R., in Electrochemical Methods: Fundamentals and Applications, 2nd Ed., Wiley, NJ, USA 2000.
33. Laviron, E.; J. Electroanal. Chem. 1979, 101, 19.
34. Alderton, A. L.; Faustman, C.; Liebler, D. C.; Hill, D. W., Biochemistry 2003, 42, 4398.

35. Mancini, R. A.; Ramanathan, R., Meat Science 2008, 78, 529.

36. Ramanathan, R.; Mancini, R. A.; Dady, G. A.; Van Buiten, C. B., Meat Science 2013, 93, 888.

37. Mikkelsen, A.; Skibsted, L. H., Z Lebensm Unters Forsch 1992, 194, 9.

CHAPTER V

SPECIES-SPECIFICITY IN MYOGLOBIN OXYGENATION AND REDUCTION POTENTIAL PROPERTIES

5.1 Introduction

The characteristic bright cherry-red color of beef is the primary determinant that influences consumers' decision to purchase meat.[1] Myoglobin is the protein primarily responsible for meat color, and it can exist in three different forms; namely deoxy-, oxy, or metmyoglobin. Myoglobin consists of a heme ring surrounded by globin. The iron present in the heme has six coordination sites, of which, four are occupied by protoporphyrin ring, the fifth by His93 residue, and the sixth site by ligands such as oxygen, water, or carbon monoxide. The ligand attached to the central heme and the valence state of iron determine meat color. In deoxymyoglobin, heme is in the ferrous state and no ligand is attached. Oxygen binding to ferrous heme results in the formation of oxymyoglobin. However, oxidation of oxy- and deoxymyoglobin leads to metmyoglobin formation.[2] Hence, processes that can promote oxymyoglobin formation (oxygenation) and metmyoglobin reducing activity can influence meat color.

Meat has an inherent capacity to limit myoglobin oxidation by a process called metmyoglobin reducing activity. To date, research has been focused on the role of enzymes, mitochondria, and NADH levels in metmyoglobin reducing capacity.[2] The ability of the heme to undergo reduction and/or oxygen binding ability and amino acid sequence also can affect meat color.

The application of electrochemical methods will help to investigate the changes in the microenvironment of heme at the active site of myoglobin.[3] Thus, characterizing the interrelationship between myoglobin reduction potential and oxygen binding properties will increase our knowledge related to meat color.

Previous research reported that myoglobin oxidation is species-specific and it depends on the primary amino acid sequence.[4] More specifically, the number of histidine residues in the myoglobin of meat-producing livestock species can influence myoglobin redox stability.[22] The amino acid composition can affect the three-dimensional structure, hence the ability of heme to an accept an electron or oxygen. Nevertheless, we are not aware of any report detailing the species-specific effects on myoglobin reduction potential and oxygen binding capacity. Therefore, the objective of the current study was to compare the myoglobin oxygenation and reduction potential properties of bovine and porcine myoglobins using electrochemical methods in-vitro.

5.2 Materials and methods

5.2.1 Materials and chemicals

High-purity graphite (HPG) disc electrodes (geometric area 0.2 cm^2) were purchased from McMaster-Carr (Atlanta, GA). Silicon carbide (SiC) paper, monosodium hydrogen phosphate ($NaH_2PO_4.H_2O$), disodium hydrogen phosphate (Na_2HPO_4) and sodium chloride (NaCl) were purchased from Sigma-Aldrich (St. Louis, MO). All chemicals were of analytical grade or greater purity.

5.2.2 Myoglobin isolation

Ammonium sulfate precipitation and gel-filtration techniques were used to isolate myoglobin from porcine and bovine heart.[6] Briefly, beef and porcine cardiac muscle devoid of fat and connective tissue was homogenized in buffer (10 mM Tris-HCl, 1 mM EDTA, pH 8.0, 4 °C) and centrifuged at 5000 x g for 10 min. The supernatant was brought to 70% ammonium sulfate saturation, and the resulting solution was stirred for 1 h at 4 °C and then centrifuged at 18,000 x g for 20 min. The supernatant was then saturated with ammonium sulfate (100%) and centrifuged at 20,000 x g for 1 h. The precipitate was re-suspended in homogenization buffer and dialyzed (3 volumes) against 10 mM Tris-HCl, 1 mM EDTA, at pH 8.0 and 4 °C for 24 h. Myoglobin was separated from hemoglobin using a Sephacryl 200-HR gel filtration column (2.5 x 100 cm) using 5 mM Tris-HCl, 1 mM EDTA, pH 8.0 as the mobile phase at 1 mL/min. The isolated myoglobin was a mixture of oxy-, deoxy-, and metmyoglobin. To limit the interference of oxidizing agents on metmyoglobin reduction, the myoglobin solution was transferred into a glass tube, and metmyoglobin was prepared by incubating myoglobin at 37 °C for 24 h. Samples were stored at −80 °C until used.

5.2.3 Electrochemical studies

5.2.3.1 Immobilization of beef and porcine Mb on high purity graphite electrodes

High purity graphite (HPG) electrodes were polished using a silicon carbide paper (P320 grit) and sonicated for 30 sec. After being rinsed in deionized water, the electrodes were dried under nitrogen. Ten microliters of purified bovine or porcine metmyoglobin (0.15 mM) were adsorbed on freshly polished HPG electrodes and incubated for 10 min at 4 °C to allow physisorption involving electrostatic and other secondary interactions.[24] The electrodes were then rinsed in deionized water to remove unbound myoglobin and the myoglobin coated HPG electrodes were used for electrochemical studies.

5.2.3.2 Myoglobin reduction potential and oxygenation measurements

Myoglobin reduction potential and oxygenation properties were determined by the methodology described by.[18] Cyclic voltammetry was used to determine the reduction potential and oxygenation properties of bovine and porcine myoglobins. Cyclic voltammetry (CV) studies were performed using a CH Instrument (CHI 1040, Bee Cave, TX) with HPG as the working electrode, platinum (Pt) wire as a counter electrode, and Ag/AgCl (1 M KCl) as the reference electrode. The cyclic voltammetry experiments were performed using 0.1 M of 10 mL mixed phosphate buffer (pH 5.6, 6.4, and 7.4) under anaerobic conditions; and these pH conditions represented postmortem muscle, dark-cutting beef, and physiological, pHs, respectively. Different pH buffers were prepared by mixing mono- and disodium hydrogen phosphate. The cyclic voltammetry experiments were performed at room temperature.

For oxygenation studies, various concentrations of oxygen (0 – 1200 μM) and nitrogen were supplied to the electrochemical cell using two mass flow controllers (Aalborg Instruments & Controls Inc., NY; model GFC17) and the percentage oxygen was converted to molar concentration using Henry's equation.[10,15] Nitrogen and oxygen gas were of ultra-high purity (Matheson Tri-Gas, Basking Ridge, NJ). Zero percent oxygen level was achieved by purging with nitrogen gas. Unless otherwise specified, all electrochemical measurements were performed in an anaerobic mixed phosphate buffer (0.1 M containing 0.15 M NaCl, at pH 5.6, 6.4, or 7.4,) under a nitrogen atmosphere. To investigate the oxymyoglobin formation constants at pH 5.6, 6.4, and 7.4, electrochemical Michaelis-Menten kinetics were employed.[7] The formation of an oxymyoglobin (Fe^{II}-O_2) complex upon the reduction of metmyoglobin in the presence of oxygen gives rise to catalytic currents in proportion to oxygen concentration (due to the reduction of formed Fe^{II}-O_2 on the electrode surface at the negative potential region). The greater the oxygen binding, the larger is

the resulting current. The relationship between oxymyoglobin reduction current and concentration of oxygen fits well in the Michaelis-Menten equation. The following formula was used to determine the myoglobin affinity for oxygen.

$$I_{cat} = \frac{nFA\Gamma k_{cat} C_s}{C_s + K_M}$$

Where n is the number of electrons in the reaction (n=2), F is faraday's constant, A is the electrode area (0.2 cm^2), Γ is the electroactive amount (mol cm^{-2}) of protein on an electrode, C_s is the concentration of oxygen, and K_M is the oxymyoglobin formation constant or Michaelis-Menten constant. K_M indicates the affinity of oxygen to bind with the reduced heme; a lower number indicates greater oxygen affinity. I_{cat} is the catalytic property of the enzyme when it reacts with the substrate. It increases when the substrate (O_2) binds to myoglobin in its reduced state. kcat is a catalytic constant also called the turnover number. The turnover number of an enzyme (myoglobin) is the number of substrate molecules (O_2) that are converted to product per unit time when the enzyme (myoglobin) is fully saturated with substrate (O_2).

A range of 0 to -0.6 V was applied to the myoglobin containing electrodes for reduction potential studies. The respective buffer was purged with nitrogen gas to attain zero oxygen concentration. Cyclic voltammetry was performed at different pH conditions to obtain reduction and oxidation peak potentials. The electrode was rotated (Eco Chemie Autolab rotator with a motor controller, Metrohm Inc., USA) at a rate of 2000 rpm to get steady state conditions. A lower number indicates myoglobin has greater reduction potential or a tendency to get reduced quickly.

5.2.4 Myoglobin modeling

The structure of the bovine (Bos taurus) myoglobin was predicted using the structure of porcine oxy-myoglobin form (protein data bank id: PDB 1 MNO), a homolog, for which the 3dimensional structure has been determined by X-ray diffraction method.[12]

This homology-based modeling was conducted using the Iterative Threading Assembly

Refinement (I-TASSER) server.[23,28,29] This homology-based modeling study with I-TASSER involves three steps: template identification from the PDB library, assembly of iterative structures, and structure-based function annotation. I-TASSER identifies the homologous structure models from the PDB4 using a Local Meta-Threading-Server algorithm.[25] The secondary structure of the target protein was predicted based on sequence information from the Protein Secondary Structure PREDiction (PSSpred) algorithm.[28] The lowest free energy conformations were determined by SPICKER (a clustering approach to identify near-native protein folds.34 Refinement of the low free energy conformations was done by using FG-MD.[31,32] Prediction of the ligand-binding site of the target protein was made by the COACH algorithm.[27]

The distance between Nε of the His 64, His 93 and His 97 and the iron and oxygen molecule of the heme group in the crystal structure of porcine myoglobin (PDB: 1MNO) was calculated using PyMOL (version 1.8). The distance between Nε of the His 64, His 93 and His 97 and the iron molecule of the heme group in the predicted structure of bovine myoglobin was also determined using PyMOL.

5.2.5 Statistical analysis

The experimental protocol was a completely randomized design (n = 6). The fixed effects include pH, species, and their interaction. Type-3 tests of fixed effects were performed using the MIXED Procedure of SAS (Version 9.1, SAS Institute Inc. Cary, NC). Least squares means for protected F-tests ($P < 0.05$) were separated by using the pdiff option (least significant differences) and were considered significant at $P < 0.05$.

5.3 Results

5.3.1 Effects of pH and species on oxygenation properties

For oxygenation studies, 0 – 1600 µM of oxygen was allowed to bind with myoglobin at pH 5.6, 6.4, or 7.4. A pH species interaction resulted for oxygenation properties (P = 0.04; Table 1). Porcine myoglobin had a greater oxygen affinity than beef myoglobin at the same pH (P = 0.04; Figure 1 and Table 1). The formation of oxymyoglobin results in a catalytic current. Figure 1 represents oxymyoglobin formation with different levels of oxygen. The relationship between oxygen concentration and the resultant current followed the Michaelis-Menten kinetics data. The numbers in the Table 1 were derived from the Michaelis-Menten kinetics data using a K-graph software. Kinetic parameters (K_M and k_{cat}) were extracted from Michaelis-Menten figure data. A lower K_M value indicates a greater affinity for oxygen binding to myoglobin at a given pH condition. The homology-based myoglobin modeling indicates that the porcine myoglobin has a shorter distance between distal histidine and heme than bovine (Table 2 and Figure 2).

Table 1. Effects of pH and species on oxygenation property1 on porcine and bovine myoglobins

Trait		Oxygen affinity (µM)[1]	SE	*P*-value
a) pH effect	pH 5.6	852.4	29.4	0.0002
	pH 6.4	591.2		
	pH 7.4	749.5		
b) Species effect	Beef	851.4	24.0	< 0.0001
	Pork	610.2		
c) pH x species effect	pH 5.6, beef	932.4[d]	41.2	0.0420
	pH 5.6, pork	772.4[bc]		
	pH 6.4, beef	778.4[c]		
	pH 6.4, pork	404.5[a]		
	pH 7.4, beef	844.0[cd]		
	pH 7.4, pork	655.0[b]		

a-dLeast square means with different superscripts significantly differ (P < 0.05). 1Michaelis-Menten constants (K_M) indicate the oxygen affinity in micromolar. Lower KM value indicates a greater affinity for oxygen binding to Mb at a given pH condition. SE indicates the standard error.

Table 2. Comparison of distance (in Angstrom) from proximal and distance histidine to heme iron in bovine and porcine myoglobins

Distance measured	Bovine	Porcine
His64 N_ε- Fe	5.6	4.3
His64 N_ε - oxygen	**	2.6
His93 N_ε- Fe	2.2	2.2
His97 N_ε- Fe	5.5	5.4

5.3.2 Effects of pH and species on reduction potential properties

The effect of pH was significant for the myoglobin reduction potential (P < 0.0001; Table3). At pH 5.6, the myoglobin reduction potential was -306.3 mV compared with -362.8 mV at pH 7.4 (P < 0.0001). The reduction potential value provides information about the ability of heme within myoglobin to accept electrons. Myoglobin redox potentials shifted more negative with increasing pH from 5.6 to 7.4, indicating a proton-coupled electron transfer process. The reduction potential values demonstrated no differences between species (P = 0.51) and also for species x pH interaction (P = 0.91).

Table 3. Effects of pH and species on reduction potential1 properties on porcine and bovine myoglobins

Trait		Reduction potential (mV)	SE	*P*-value
a) pH effect	pH 5.6	-306.3[a]	2.3	< 0.0001
	pH 6.4	-319.2[b]		
	pH 7.4	-362.8[c]		
b) Species effect	Beef	-328.6	1.8	0.5162
	Pork	-330.3		
c) pH x species effect	pH 5.6, beef	-305.2	4.6	0.9185
	pH 5.6, pork	-307.4		
	pH 6.4, beef	-319.3		
	pH 6.4, pork	-319.0		
	pH 7.4, beef	-361.4		
	pH 7.4, pork	-364.5		

a-cLeast square means with different superscripts significantly differ (P < 0.05). SE indicates the standard error.

5. 4 Discussion

Meat is a complex system; various processes and organelles such as mitochondria, lipid oxidation, and microorganisms compete for oxygen. Hence, to study oxygen binding properties specifically to myoglobin in a meat system might be challenging. We utilized an electrochemical approach to understanding the biochemical basis of oxygen binding to myoglobin in vitro. Various research has employed cyclic voltammetry to study protein functionality and successfully extrapolated the effects under physiological conditions.[7,20]

The mechanistic basis for species-specific effects of oxygen binding on myoglobin is not clear. In the current study, porcine myoglobin had greater oxygen affinity conditions than bovine

myoglobin. Porcine and bovine myoglobin share 88% amino acid sequence homology (www.expasy.org; Table 4). Further, the differences in amino acid sequence between species could be partially responsible for changes in oxygen affinity. The amino acid sequence can affect the net charge of a protein and its affinity for oxygen. Marcinek et al. (2001) reported that oxygen binding depends on the amino acid sequence surrounding the heme pocket. In addition, the primary amino acid sequence can affect the tertiary structure, which in turn can influence interactions with ligands and also the volume of the heme cavity.[22] In support, Bunn (1971) reported that porcine hemoglobin has greater oxygen affinity than bovine hemoglobin, due to differences in amino acid composition. Furthermore, variation in the primary structure was responsible for species-specific effects of secondary lipid oxidation products on myoglobin redox stability.[22] For example, porcine myoglobin contains 9 histidine residues, while bovine myoglobin contains 13 such residues. The lower the number of nucleophilic histidins in porcine myoglobin than bovine is responsible for its greater redox stability against 4-hydroxy-2-nonenal. More specifically, 4-hydroxy-2-nonenal can preferentially bind with nucleophilic histidins that are available for reaction.

In addition to differences in the number of histidine residues, differences in distances between the distal histidine and the heme can influence oxygen binding. The distal histidine plays a significant role in stabilizing the oxygen bound to heme. A shorter distance between the distal histidine and the heme in porcine myoglobin might have favored oxygen binding to the heme compared with bovine myoglobin.

At pH 5.6, the net charge of bovine myoglobin and porcine myoglobin were, 12.4 and 8.8, respectively (http://protcalc.sourceforge.net/). A greater positive charge could be less favorable for oxygen to bind with beef myoglobin. Although the exact mechanism is not clear, we speculate from medical research. More specifically, hemoglobin at a lower pH (greater positive charge) has a lower affinity for oxygen due to the Bohr effect (Benesch and Benesch, 1961).

However, in myoglobin, a lower pH minimizes heme-apomyoglobin contact.[13] This support the current research that the oxygen affinity was lower at pH 5.6 compared with 6.4 and 7.4 within a species. Previous research using steaks reported greater oxygenation or bloom in pork than beef (Hass and Brazlter, 1965). Greater oxygen affinity to porcine myoglobin, in part, could be responsible for more bloom in pork than beef. Porcine myoglobin has been crystallized, but, bovine myoglobin has not been crystallized yet.[3] Hence, it was not possible to compare the amino acid sequence surrounding the heme cavity. Interestingly, in the current study, the oxygen affinity was greater at pH 6.4 than pH 5.6 and 7.4 for both species. Distal histidine plays a major role in stabilizing ligands such as oxygen. The pKa of histidine is 6.1. Since the pKa is close to pH 6.4 compared with pH 5.6 and 7.4, a lower charge difference might have favored oxygenation.

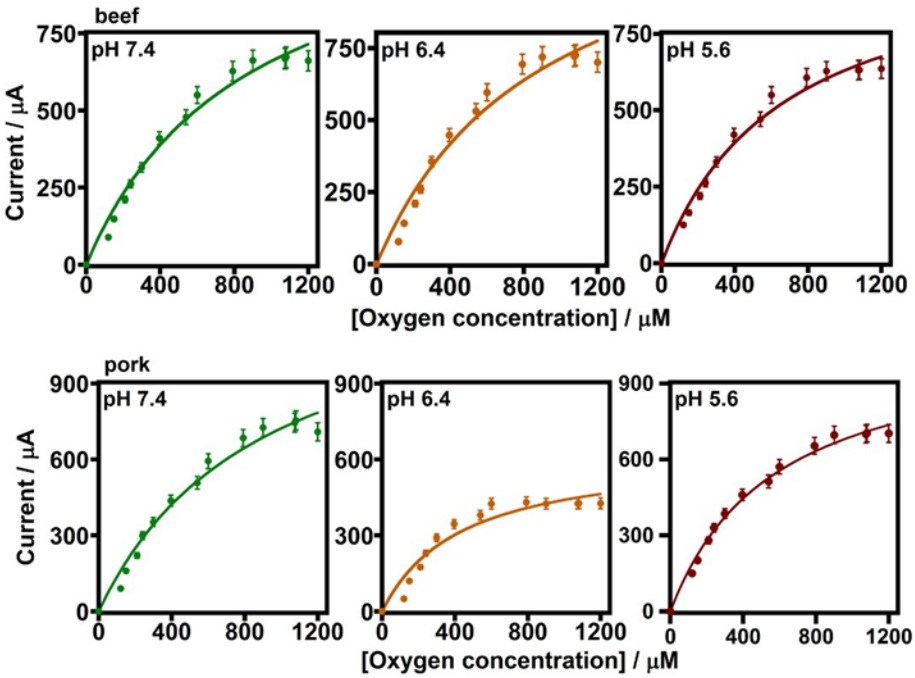

Figure 1. The Michaelis - Menten kinetics1 observed for the reduction currents of beef and pork myoglobin versus O2 concentration in pH 5.6, 6.4, and 7.4

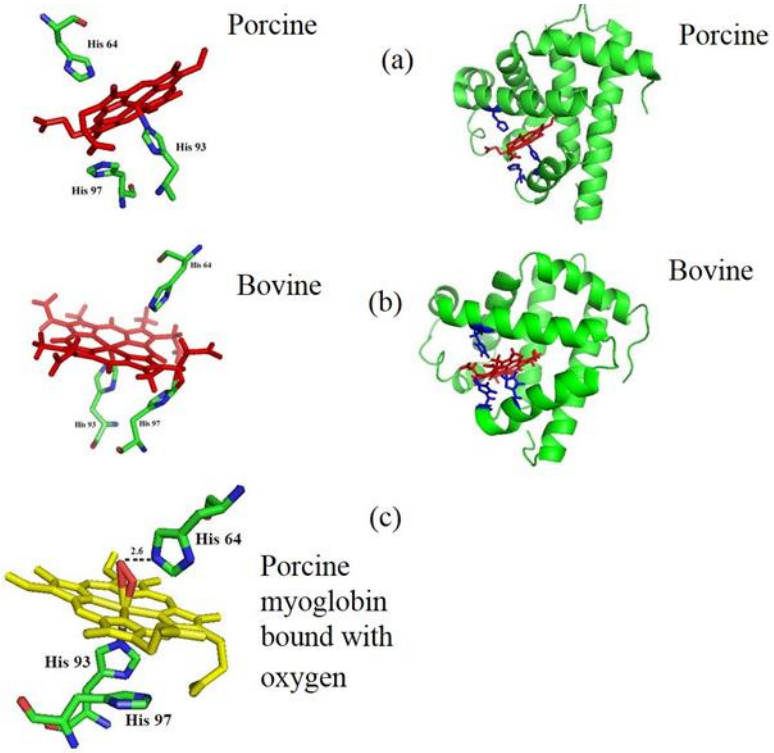

Figure 2. Three-dimensional representation of porcine and bovine myoglobins

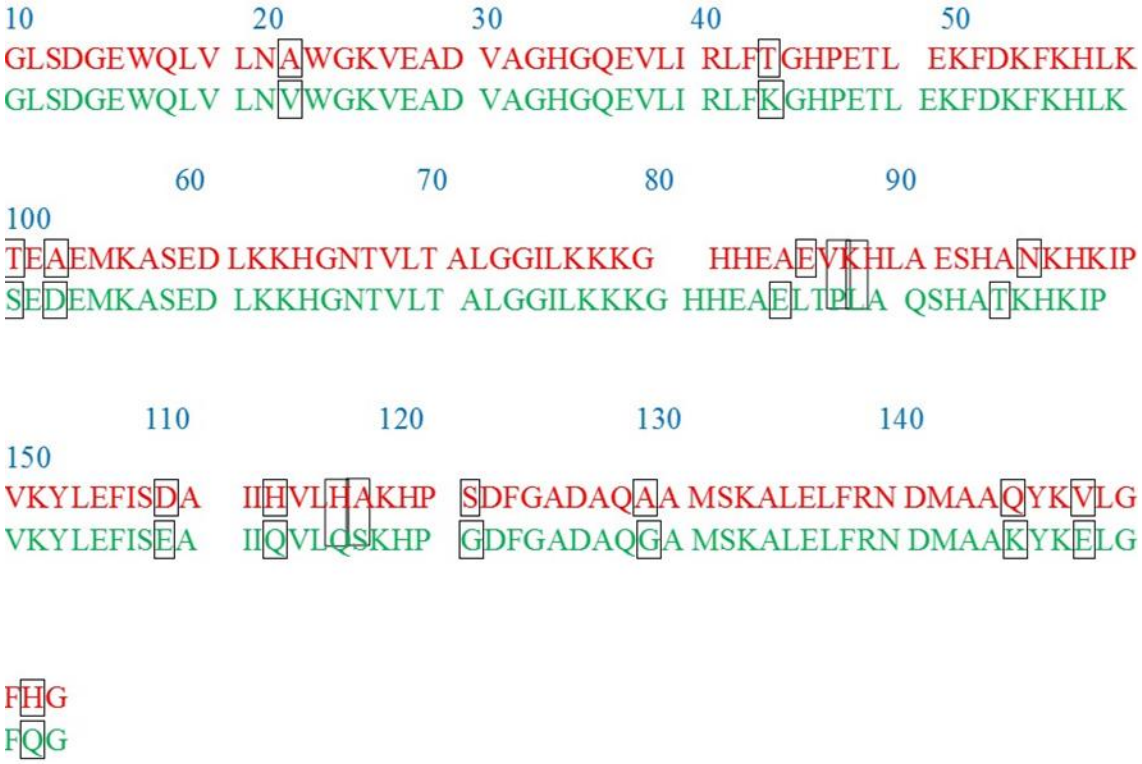

Figure 3. Comparison of amino acid sequences of porcine and bovine myoglobin. Differences in amino acids are represented by a text box. The first row represents bovine myoglobin and the second row represents porcine myoglobin

In the present study, there was no significant effect of species on reduction potential. The results suggest that there were no differences between species at a particular pH to accept an electron. However, there was a significant effect of pH on the reduction potential. A pH of 7.4 favored reduction more than a pH of 6.4 or 5.6. Previous research using equine myoglobin also reported a greater metmyoglobin reduction at pH 7.4.[18] Greater metmyoglobin reducing activity at an elevated pH in meat, can in part, and can be attributed to the ability of heme to accept an electron more quickly than normal pH. Metmyoglobin reduction changes with conditions and also depends on the type of system used. For example, Elroy et al. (2015) reported that porcine and bovine myoglobin have different non-enzymatic metmyoglobin reduction capacity. The enzymatic reaction involves three-dimensional binding of co-factors and proteins, which aid in electron

transfer to ferric heme. However, application of a potential to a graphite electrode will move an electron directly to heme.

5.5 Conclusions

A meat matrix is composed of various biomolecules; hence to study myoglobin functional properties can be challenging. The current study suggests that cyclic voltammetry is a useful tool to characterize myoglobin reduction potentials and oxygenation properties. Oxygen binding to myoglobin is species-specific. Further, homology-based modeling helps to explain the speciesspecific variation in myoglobin properties. The results indicate that cyclic voltammetry can be a valuable tool to understand meat biochemical properties such as the effects of pH on bloom, effects of temperature on myoglobin reduction potential, and the role of lipid oxidation products on myoglobin redox stability.

5.6 REFERENCES

1. AMSA. 2012. Meat color measurement guidelines. 2nd ed. Am. Meat Sci. Assoc., Chicago, IL. Benesch, R. and Benesch. R. E. 1961. The Chemistry of the Bohr Effect. J. Biolo. Chem. 236, 405410.
2. Bunn, H.F., Science. 1971 172: 1040–1050.
3. Cai, H.; Tatiyaborworntham, N.; Yin, J.; Richards. M. P., J. Food Sci. 2016 81: 42-48.
4. Dutta, S.; Berman, H. M.; Bluhm, W. F., Curr Protoc Bioinform. 2007, 20, 1.9.1–1.9.24.
5. Elroy, N. N.; Rogers, J.; Mafi, G. G.; VanOverbeke, D. L.; Hartson, S. D.; Ramanathan. R., Meat Sci. 2015 105: 108-113.
6. Faustman, C.; Phillips, A. L., 2001.Current protocols in food analytical chemistry. New York: Wiley (Ch. F3 Unit F3.3).
7. Guto, P. M.; Rusling, J. F., J. Physical Chem. 2005. 109: 24457- 24464.
8. Hass, M. C.; Brazlter. L. J., J. Food Sci. 1965 30: 64-68.
9. Jayasingh, P.; Cornforth, D. P.; C. E. Carpenter,; Whitter. D., Meat Sci. 2001 59:317–324.
10. Kavanaugh, M. C.; Trussell. R. R., J. Am. Water Works Assoc. 1980 72, 684–692.
11. Kim, Y. H., Hunt, M. C.; Mancini, R. A.; Seyfert, M., Loughin, T. M.; Kropf, D. H.; Smith. J. S., J. Agric. Food Chem. 2006 54: 7856−7862.
12. Krzywda, S.; Murshudov, G. N.; Brzozowski, A. M.; Jaskolski, M.; Scott, E. E.; Klizas, S. A.; Gibson, Q. H.; Olson, J. S.; Wilkinson, A. J., Biochem. 1998 37: 15896-15907.
13. La Mar, G. N.; Budd, D. L.; Sick, H.; Gersonde, K., Biochimica Biophysica Acta (BBA) – Protein Stru. 1978 537, 270-283.
14. Lanari, M. C.; Cassens. R. G., J. Food Sci. 1991 56: 1476–1479.

15. Loomis, A. G. 1928. Solubilities of gases in water. In E. W. Washburn, C. J. West, N. E. Dorsey, F. R. Bichowsky, and A. Klemenc, Physics, Chemistry and Technology, 1928 255-261.

16. Mancini, R. A.; Hunt, M. C., Meat Sci. 2005 71: 100–121.

17. Marcinek, D. J., Bonaventura, J.; Wittenberg, J. B.; Block. B. A., The American J. Phy.-Regu, Integ. and Comp. Physio. 2001 280: 1123-1133.

18. Nerimetla, R., Walgama, C.; Ramanathan, R.; Krishnan. S., Electroanalysis. 2014 26: 675 – 678.

19. Protein Calculator v3.4 http://protcalc.sourceforge.net/

20. Qian, Y., Xu, X.; Wang, Q.; Wu, P.; Zhang, H.; Cai. C., Phys. Chem. Chem. Phy. 2013 15: 16941 -16948.

21. Roy, A.; Kucukural, A.; Zhang. Y., Nature Proto. 2010 5: 725-738.

22. Suman, S. P.; Faustman, C.; Stamer, S. L.; Liebler. D. C., 2007 7: 628–640.

23. The PyMOL Molecular Graphics System, Version 1.8 Schrödinger, LLC.

Tang, J., Faustman, C.; Mancini, R. A.; Seyfert, M.; Hunt. M. C., J. Agric. Food Chem. 2005 53: 5449−5455.

24. Van Dyke, B. R., Saltman, P.; Armstrong. F., J. Am. Chem. Soc. 1996 118: 3490 -3492.

25. Wu, S.; Zhang. Y., Nucleic Acids Resear. 2007, 35: 3375–3382.

26. Xu, D., and Zhang, Y. Biophys J. 2011, 101: 2525–2534.

27. Yang, J., A. Roy, and Y. Zhang. Bioinform. 2013. 29: 2588–2595.

28. Yang, J., R. Yan, A. Roy, D. Xu, J. Poisson, and Y. Zhang. 2015. Nature Meth. 12: 7-8.

29. Yang, J., and Y. Zhang., Nucleic Acids Resear. 2015, 43: 174-181.

30. Yin, S., Faustman, C.; Tatiyaborworntham, N.; Ramanathan, R.; Maheswarappa, N. B.;

31. Mancini, R. A.; Joseph, P.; Suman, S. P.; Sun. Q., J. Agric. Food Chem. 2011. 59: 12198–12203.

32. Zhang, J., Liang, Y.; Zhang. Y., Structure. 2011 19: 1784–1795.

33. Zhang, Y. I-TASSER server for protein 3D structure prediction. BMC Bioinformatics. 2008 9: 40.

34. Zhang, Y.; Skolnick. J., J. Comput. Chem. 2004 25: 865–871.

CHAPTER VI

CONCLUSIONS

In Chapter II, the electrocatalytic pathway of CPR-mediated electrocatalysis operative in the CYP+CPR containing bactosomes and the favorable effect of catalase in enhancing the electrocatalytic product yield of CYP+CPR bactosomes were determined. New mechanistic insights about the electrocatalytic function of CYP bactosomes with CPR were obtained. The simplicity and cost-effective nature of the designed bioelectrodes is useful for drug metabolism assays, biosensing, and biocatalytic applications.

In Chapter III, designed liver microsomal bioreactors on carbon nanostructured electrodes offered direct electrochemical communication between the microsomal proteins and MWNT-modified electrodes, direct electrocatalysis, sufficient catalytic stability, and reusable features.

In Chapter IV, we observed direct electrochemical communication between the microsomal proteins combined with MNP modified EPG or) electrodes. Chronoamperometry studies showed that MNP/HLM electrodes displayed good enzyme activity, direct electrocatalysis and strong substrate affinity. MNP/HLM electrodes are promising for cost-effective development of microsomal drug metabolite bioreactors for new drugs in development.

We have tested three pH conditions, relevant to the physiological, stress animal muscle and postmortem meat (Chapters V and VI). The observed greater electrochemical metmyoglobin

reduction and stronger oxymyoglobin formation constant at pH 7.4 correlated well with the bright-red color of a fresh meat at this pH over acidic pH. Understanding the redox-processes of meat by electrochemical methods is valuable in designing novel tools to predict meat color and quality.

VITA

Rajasekhara Reddy Nerimetla

Candidate for the Degree of

Doctor of Philosophy

Thesis: VOLTAGE-DRIVEN BIOCATALYSIS BY MEMBRANE-BOUND LIVER ENZYMES

Major Field: Chemistry

Biographical:

Education:

Completed the requirements for the Doctor of Philosophy in Chemistry at Oklahoma State University, Stillwater, Oklahoma in July, 2017.

Completed the requirements for the Master of Science in Chemistry at Banaras Hindu University, Varanasi, Uttar Pradesh, India in 2010.

Completed the requirements for the Bachelor of Science in Chemistry at Sri Krishnadevaraya University, Anantapur, India in 2007.